This is a repository copy of *The influence of relative fluid depth on initial bedform dynamics in closed, horizontal pipe flow*.

White Rose Research Online URL for this paper:
http://eprints.whiterose.ac.uk/114121/

Version: Accepted Version

Article:

Accepted Manuscript

The influence of relative fluid depth on initial bedform dynamics in closed, horizontal pipe flow

Hugh P. Rice , Michael Fairweather , Timothy N. Hunter ,
Jeffrey Peakall , Simon R. Biggs

Please cite this article as: Hugh P. Rice , Michael Fairweather , Timothy N. Hunter , Jeffrey Peakall , Simon R. Biggs , The influence of relative fluid depth on initial bedform dynamics in closed, horizontal pipe flow, *International Journal of Multiphase Flow* (2017), doi: 10.1016/j.ijmultiphaseflow.2017.03.007

Highlights

- Particle bed depth in horizontal pipe flow measured with acoustic backscatter.

- Evolution of bedforms over time observed and categorized into five types.

- Bedform type influenced by initial flow rate, relative fluid depth.

- Observed bedform evolution supports distinct ripple and dune modes.

- Universal scalings for pipe, channel and environmental flows proposed.

The influence of relative fluid depth on initial bedform dynamics in closed, horizontal pipe flow

Hugh P. Rice[*1], Michael Fairweather[1], Timothy N. Hunter[1], Jeffrey Peakall[2] and Simon R. Biggs[1,3]

[1] School of Chemical and Process Engineering, University of Leeds, Leeds LS2 9JT, UK

[2] School of Earth and Environment, University of Leeds, Leeds LS2 9JT, UK

[3] Current address: Faculty of Engineering, Architecture and Information Technology, University of Queensland, St Lucia QLD 4072, Australia

* Correspondence to h.p.rice@leeds.ac.uk

Abstract

Measurements of time-dependent bedforms produced by the deposition of solid plastic particles in two-phase liquid-solid flows were performed using a novel ultrasonic echo method and *via* video image analysis in a 100-liter, closed-pipe slurry flow loop. Results are presented for the settled bed thicknesses over a range of nominal flow rates and initial bed depths and are combined into several phase diagrams based on various combinations of parameters, with the bedforms categorized into five types. The novel observation is made that the type of bedform that arises depends on both the flow rate and the initial relative bed or fluid depth, with both ripples and dunes being observed in the same system and in a single experiment. In addition, the critical Shields number at incipient particle motion is measured to be θ_{sc} = 0.094 ± 0.043, hysteretic behavior is observed, and the evolution and scaling of each time-dependent type of bedform is analyzed in detail and compared against several expressions for initial and equilibrium dimensions from the literature. A number of universal scalings for bedforms in any type of conduit are proposed with a view ultimately to unifying the observations of bedforms in pipes with those in channels and natural flows.

1   Introduction

The hydraulic implications of moving and stationary particle beds in low-velocity multiphase

2

engineering flows have received relatively little research attention, despite considerable interest in understanding critical deposition and stratification in higher velocity flows (e.g. Rice *et al.*, 2015a; Rice *et al.*, 2015b). The importance of lower-velocity bedform dynamics is, however, also of critical concern, whether it be in terms of the enhancement or inhibition of solids transport, flow field properties, modification of effective surface roughness, conduit wear/corrosion, or the likelihood of solid plug formation and subsequent blockages. In the case of nuclear engineering, for example, it is not known whether such flows are likely to affect the radiative environment in terms of heat formation and radiochemical interactions with the conduit materials. In the case of civil engineering, it is equally unclear whether bedforms may hinder the ability of waste and run-off water systems to function efficiently (Banasiak and Tait, 2008; Banasiak and Verhoeven, 2008; Lange and Wichern, 2013; Matoušek, 2005; Skipworth *et al.*, 1999).

Despite the lack of research on mobile beds in engineering transport systems (either open or closed conduits), bedforms are ubiquitous in nature in both sub-aqueous (water-driven) and aeolian (air-driven) environments, and their laboratory analogs have been studied extensively by earth scientists in open and closed rectangular channels. As a result there is a large, mature canon of literature describing their behavior in natural and laboratory environments (see, for example, the reviews of Baas *et al.*, 2016; Best, 2005; Charru *et al.*, 2013; Coleman and Nikora, 2011; García, 2008). Bedforms can very broadly be grouped into three regimes: lower/sub-critical (lower plane beds, ripples, ripples on dunes, dunes), transitional (washed-out dunes) and upper or supercritical (upper plane beds, antidunes, chutes and pools) (Graf, 1984; Simons and Richardson, 1961); here the focus is on ripples and dunes.

In the case of open channel and environmental systems, ripples and dunes form at low flow rates, provided generally that particle diameter, $d < 0.7$ mm for ripples and $d > 0.1$ mm for dunes (Leeder, 2011, p. 132-137), all configurations of which prograde (*i.e.* progress downstream). Ripples form when the particle size and shear Reynolds number are both small (Raudkivi, 1997). Importantly, their equilibrium sizes scale with grain size, but are *independent* of flow depth, whereas those of dunes scale with flow depth (Charru *et al.*, 2013; Van Rijn, 1989). More specifically, van Rijn (1984c) also states that while both ripple heights and lengths are much smaller than the flow depth, dune lengths can be much greater than that depth.

There has been much debate over how the formation of ripples, dunes or other bedforms eventuate from a set of flow, particle and environmental conditions (e.g. Charru *et al.*, 2013; Colombini and Stocchino, 2011; Fourrière *et al.*, 2010). Most workers agree that ripples initially

arise from a linear instability, however there is debate on whether dunes arise directly from a linear instability, or form through non-linear processes from progressive growth of ripples, referred to as pattern coarsening (e.g. Charru *et al.*, 2013; Colombini and Stocchino, 2011; Fourrière *et al.*, 2010; Kennedy, 1963; Richards, 1980). Here these arguments are briefly reviewed, starting with the stability analysis of bedforms that considers how an initial (sinusoidal) perturbation applied to a planar bed of particles will be amplified or damped. In general, when a bed surface is perturbed, there are two possibilities according to whether the lag distance, δ, caused by the competition between the local sediment transport rate and the velocity at the bed is positive or negative (Engelund and Fredsøe, 1982; García, 2008). If the bed is stable ($\delta > 0$) then the perturbation is attenuated by changes in the flow and sediment transport rate, while if the bed is unstable ($\delta < 0$) the perturbation grows, resulting in wave-like bedforms (dunes, ripples, *etc.*).

In a linear stability analysis of an erodible bed in the presence of a free water surface, Kennedy (1963) incorporated the lag distance, δ, and categorized the resulting bedforms as dunes, plane beds or anti-dunes depending on the value of $k\delta$ and the flow depth, where k is the bedform wavenumber, but the model did not predict ripples. Richards later (1980) extended a model by Engelund (1970) and considered the effects of turbulence more thoroughly, finding two modes of growth corresponding to dunes and ripples. However, Charru and Mouilleron-Arnould (2002) note that these and other models tend to underpredict the wavelength of instabilities when compared to most experimental data. Colombini and Stocchino (2011) have further extended this approach and conclude that both ripples and dunes do indeed arise as primary instabilities, rather than dunes forming as a result of "coarsening" of ripples. In contrast, Fourrière *et al.* (2010) and Charru *et al.* (2013) have argued that dunes do not arise directly from an instability, but rather by progressive growth (coarsening) of ripples over time. Ripples have been observed to grow non-linearly after initial formation, through merger of bedforms since smaller bedforms travel faster than larger ones (Coleman and Melville, 1994; Fourrière *et al.*, 2010).

The engineering implications of bedforms in closed conduits are not clear. It is not known, for example, whether time-varying bedforms in pipes increase or decrease the likelihood of blockages. However, it is reasonable to assume that the morphology of bedforms will influence the mean (and in turbulent flows, fluctuating) velocity fields and particle flux strongly. It is surprising, then, how few studies of bedforms in equivalent phase spaces in closed-conduit systems exist (for example, Edelin *et al.*, 2015; Kuru *et al.*, 1995). The authors are aware of just 12 such studies, as summarized in Table I, where the Reynolds number, Re_{pipe}, is defined as

4

follows:

$$\mathrm{Re}_{\mathrm{pipe}} = \frac{U_{ave}D}{\nu},$$ [1]

where U_{ave} is the mean axial flow velocity, D is the conduit diameter and ν is the kinematic viscosity of the fluid phase.

Table I: Studies of bedforms in closed conduits.						
Reference	Conduit	Dimensions (mm)	Mean flow velocity (m s^{-1}) or Re	Particle size (mm)	Particle density (10^3 kg m^{-3})	No. runs
Ismail (1952) (in Acaroglu, 1968, p. 113)	Rectangular	27 × 7.6	8.93-1.50	0.091, 0.147	2.65	60
Thomas (1964)	Pipe	25.1, 100.4	0.12-0.37	0.05-0.507	1.09, 2.65	~75
Wilson (1965) (in Acaroglu, 1968, p. 113)	Rectangular	9.37 × 9.37	0.69-2.03	0.710	2.65	67
Kriegel and Brauer (1966) (in Acaroglu, 1968, p. 113)	Pipe	53.5	0.72-2.27	1.15-1.90	1.38-1.43	129
Acaroglu (1968)	Pipe	76.2	0.56-6.50	2.00, 2.78	2.67	223
Nakagawa and Tsujimoto (1984)	Rectangular	310 × 75	0.507, 0.676	0.07	Unknown (sand)	2
Takahashi *et al.* (1989)	Pipe	49.7	1.2-1.6	2.18, 3.06	2.74	~40
Kuru *et al.* (1995)	Pipe	31.1	Re = 1,800-12,000	0.1, 0.3	2.4	n/a
Simkhis *et al.* (1999)	Pipe	40	0.3	3	1.24	1
Coleman *et al.* (2003)	Rectangular	300 × 100	0.263-0.703	0.11, 0.87	2.65	12
Ouriemi *et al.* (2009)	Pipe	30	Re = 10^{-1}-10^4	0.132, 0.193, 0.538	2.490, 1.177, 1.070	n/a
Edelin *et al.* (2015)	Pipe	30	Re < 15,000	0.756	0.907	n/a

Of the studies listed in Table I, four were performed in rectangular channels and the rest in cylindrical pipes. Coleman *et al.* (2003) reviewed the majority of these studies and highlighted that available data on the generation and development of bedforms in closed-conduit flows are limited.

Ouriemi *et al.* (2009) classified time-dependent bedforms observed in pipe flow as either "small", "vortex" or "sinuous" dunes, the latter being observed only in turbulent flow. However, it is important to note that, in the sedimentology literature, "sinuous" refers to the latitudinal shape of dunes rather than the longitudinal shape, and the bedforms observed by Ouriemi *et al*. (2009) were strictly ripples, not dunes, based on their observed dimensions and the diameter of

the particles used. They also presented a phase diagram of Re against Ga$(H/d)^2$, where H is the fluid depth (*i.e.* $H = D – h$, where D is the pipe diameter and h is the bed depth), d is the particle diameter and Ga is the Galilei number, which is defined as follows:

$$\text{Ga} = \frac{d^3(s-1)g}{\nu^2} = \text{Re}_p^2,$$ [2]

where s is the specific gravity of the solid phase, g is the acceleration due to gravity, ν is the kinematic viscosity of the fluid and Re$_p$ is the particle Reynolds number, defined as:

$$\text{Re}_p = \frac{d[(s-1)gd]^{1/2}}{\nu}.$$ [3]

In their phase diagram, Ouriemi *et al.* (2009) correctly predicted the threshold between a stationary and moving bed, and the development of "small dunes", according to a linear stability analysis. Additionally, they found that the behavior of two categories of bedforms ("small" and "vortex") were well separated on a plot of h_b/D against $U_{ave}t/D$, where h_b is the bedform height and t is time.

In the majority of the studies listed in Table I, only ripples or dunes (and not both) were likely to have been encountered, based on the particle diameters used in the experiments: in the cases of the studies of Kriegel and Brauer (1966), Acaroglu (1968), Takahashi *et al.* (1989) and Simkhis *et al.* (1999), only dunes; in the cases of Ismail (1952), Nakagawa and Tsujimoto (1984), Wilson (1965) and Edelin *et al.* (2015) only ripples. Coleman *et al.* (2003) used two particle types of different sizes, one that was likely to produce ripples and the other to produce dunes. It is also important to note, as Coleman *et al.* (2003) have done, that measurements of the bed dimensions were taken while the flow was stopped in the studies of Nakagawa and Tsujimoto (1984) and Kuru *et al.* (1995). It is therefore possible that flow deceleration influenced the measurements in those cases.

There are several differences between open and closed, and cylindrical and rectangular conduits that would be expected to influence the development and equilibrium dimensions of bedforms, and therefore the structure of any phase diagram that describes them. In a conduit with a circular cross-section, the flow structure may be significantly modified by the presence of a thick bed (Adams *et al.*, 2011); secondly, calculations of bulk quantities such as mass flux must take account of the variation in chord length (*i.e.* bed width at the top of the bed) with height,

although Kuru *et al.* (1995), for example, in their study of erodible beds in pipes, assumed that the asymmetrical effects of the circular pipe are not significant when the shear layer is very thin compared to the pipe diameter. These differences aside, Coleman *et al.* (2003) have stated that, although the absence of a free surface causes bedforms to develop more quickly in closed conduits, their equilibrium dimensions appear to be the same as in equivalent open-channels flows. Thomas (1964) also noted that bedforms in open, closed, natural and artificial flow geometries appear to be closely related phenomena, and thus theories should account for both system types.

Given the lack of data on bedform behavior in closed conduits and the engineering implications of the associated flow transitions, it is clearly a pressing area of research. Here the initial, non-equilibrium behavior of time-dependent bedforms in two-phase, liquid-solid flow in a horizontal pipe is investigated using a novel ultrasonic backscatter method and *via* video image analysis. The overall aim is to derive a phase diagram of bedform types, for which several categories are defined, and the thresholds delineating the types are identified.

2   Background

It is important to identify some underlying properties of ripples and dunes, which are generally identified as different kinds of bedforms of "distinctly separate scales with no gradual transition" (Coleman and Nikora, 2011). García (2008) has reviewed some common ripple and dune scalings in terms of equilibrium height, wavelength and celerity (*i.e.* rate of progradation), and states that dune *heights* satisfy the following expression:

$$\frac{h_b}{H} \leq \frac{1}{6},$$
[4]

where h_b is the bedform height and H is the fluid depth. However, this expression does not distinguish between dunes and ripples, as ripples are independent of flow depth and are smaller than dunes (Charru *et al.*, 2013). Julien and Klaassen (1995) derived the following relationship for dunes based on a compilation of laboratory and field data, which allows relative dune height to be related to particle size (d_{50}):

$$\frac{h_b}{H} = 2.5 \left(\frac{d_{50}}{H}\right)^{0.3}.$$
[5]

Van Rijn (1984a) derived a relationship that defined the critical dune height ratio in terms of the critical shear flow velocities and particle size relationship as follows (van Rijn, 1984a):

$$\frac{h_b}{H} = 0.11 \left(\frac{h_b}{H}\right)^{0.3} (1 - e^{-0.5T})(25 - T), \tag{6}$$

where T is referred to as the transport stage parameter, which is defined below:

$$T = \frac{(U'_\tau)^2 - (U_{\tau,cr})^2}{(U_{\tau,cr})^2}, \tag{7}$$

where U'_τ and $U_{\tau,cr}$ are the particle bed shear velocity and the critical bed shear velocity, respectively, and are as follows:

$$U'_\tau = \frac{g^{1/2} U_{\text{flow}}}{C'}, \tag{8}$$

$$\frac{(U_{\tau,cr})^2}{(s-1)gd_{50}} = \theta_s = \begin{cases} 0.24(d^*)^{-1} & d^* \leq 4 \\ 0.14(d^*)^{-0.64} & 4 < d^* \leq 10 \\ 0.04(d^*)^{-0.10} & 10 < d^* \leq 20 \\ 0.24(d^*)^{0.29} & 20 < d^* \leq 150 \\ 0.055 & d^* > 150 \end{cases} \tag{9}$$

where U_{flow} is the mean axial flow velocity in the flow area and d^* is the dimensionless particle size and C' is the particle Chézy coefficient, which are defined as (García, 2008; van Rijn, 1984a):

$$d^* = d_{50} \left[\frac{(s-1)g}{v^2}\right]^{1/3}, \tag{10}$$

$$C' = 18\log\left(\frac{4H}{d_{90}}\right), \tag{11}$$

and θ_s is the Shields number, a dimensionless shear stress defined as follows:

$$\theta_s = \frac{\tau_b}{gd(\rho_s - \rho_f)}, \tag{12}$$

where ρ_s and ρ_f are the solid and fluid densities, respectively, and τ_b is the bed shear stress.

Coleman and Eling (2000) and Coleman *et al.* (2003) found that the following expression for the

8

wavelength, λ_b, of initial bedforms referred to as "wavelets" fit a large number of data taken from the literature:

$$\lambda_b = 175d^{0.75}, \qquad\qquad [13]$$

with λ_b and d in millimeters, while various expressions for equilibrium bedform wavelength have been given by Julien and Klaassen (1995), Raudkivi (1997) and Baas (1993, 1994) but are not reproduced here for brevity, as the focus here is on initial bedform development.

An important consideration is the choice of scaling parameters for constructed phase diagrams. While the Shields number is quite often used (see, for example, Edelin *et al.*, 2015; Kuru *et al.*, 1995) both Ouriemi *et al.* (2009) and Edelin *et al.* (2015) found that it was inadequate to describe ripple and dune transition in pipe flows and concluded that the geometry of the flow should also be incorporated. Alternatively, both Ouriemi *et al.* (2009) and Sumer and Bakioglu (1984) found that an instability occurred at a critical value of a characteristic Reynolds number (a particle Reynolds number in the case of the former group, and a grain Reynolds number in the latter). However, Charru and Hinch (2006) delineated stable and unstable plane beds with a critical value of the Galilei number, Ga, which is defined in Equation [2] and is a measure of the ratio of gravitational to viscous forces, of which gravity tends to be stabilizing and viscosity destabilizing. As measurements of the bed critical shear stress are much more difficult in closed conduits than in open channels, use of Ga as a scaling parameter is advantageous for pipe-flow studies. Additionally, in any closed conduit, the absence of a free water surface means a no-slip condition exists at all boundaries, and anti-dunes and chutes/pools, the formation of which depends on the interaction between the bed and free water surfaces, cannot develop. The Froude number, upon which the delineation of sub- and supercritical flows is based, is defined as follows:

$$\mathrm{Fr} = \frac{U_{\text{flow}}}{(gH)^{1/2}}, \qquad\qquad [14]$$

where H is the fluid depth. Although other definitions of the Froude number exist (for example, Gillies *et al.*, 2004), the one above permits comparison of open- and closed-duct, channel and pipe flows, since U_{flow} and H can be defined unambiguously in all cases.

In contrast to Yalin (1972), Kuru *et al.* (1995) found that "sand waves" form on initially smooth beds under laminar flow and that turbulence is not required; similar observations were made

by Coleman and Eling (2000) and Coleman *et al.* (2003). However, as described in more detail later, all ripples/dunes described here developed under turbulent flow conditions.

3   Experimental method

3.1   *Particle and flow loop properties*

An off-the-shelf ultrasonic system was chosen for the present study, consisting of a *UVP-DUO* signal processor (Met-Flow, Switzerland) and a monostatic (*i.e.* emitter-receiver) transducer operating at 4 MHz. The transducer was mounted, perpendicular to the mean flow direction, on a transparent, horizontal test section of a recirculating pipe flow loop with an inner diameter of D = 42.6 mm at a distance 75 D from the nearest fitting to ensure the flow was fully developed (i.e. statistically invariant in the axial direction) at the test section. More details of the flow loop employed can be found elsewhere (Rice *et al.*, 2015a). In addition, high-quality video footage of bedform development in a single experiment was recorded with a Nikon D3100 camera and a Nikon AF Micro-Nikkor 60 mm f2.8D lens. A variable centrifugal pump was used to control the flow rate, an impeller mixer to maintain a suspension in the mixing tank (nominal capacity 100 liters, *i.e.* 0.1 m^3) and an electromagnetic flow meter to measure the flow rate, Q. The flow loop was filled with suspensions of the particle species at several nominal (weighed) concentrations, ϕ_w, with ϕ_w = 0.1, 0.5, 1 and 3% by volume, and run over a range of flow rates, as described in more detail later (Section 3.3).

Non-spherical plastic particles, the physical properties of which are summarized in Table II, were used in all the experiments and were sourced from a blast media supplier (Guyson International, Ltd., UK). A micrograph of the particle species is given in the Supplementary Material. The particle size distribution was measured with a Malvern Instruments *Mastersizer 3000* laser diffraction sizer and a Retsch Camsizer XT optical size and shape analyzer, and the density with a Micromeritics *AccuPyc 1300* pycnometer.

Table II: Physical properties of particle species used in present study.					
Trade name	Material	Particle size, *i*th percentile, d_i (µm)			Density, ρ_s (10^3 kg m^{-3})
		d_{10}	d_{50}	d_{90}	
Guyblast 40/60	Urea formaldehyde	269*	468*, 442**	712*	1.52
* Malvern *Mastersizer* 3000					
** Retsch *Camsizer XT*, based on equivalent-area diameter					

3.2   *Distance calibration and bed depth measurement*

The methods of positional calibration of the acoustic probe and bed depth measurement are as

described by Rice *et al.* (2015a) with the same flow loop. The following parameters were used in the *UVP-DUO* system software, where r is the axial distance from the active face of the transducer: r_0 and r_{max} are the minimum and maximum measurement distances, respectively, with r_0 = 5 mm and r_{max} = 50 mm; w is the width of each measurement bin and s is the separation between the central points of adjacent measurement bins, with $s = w$ = 0.37 mm. The flow radius in all runs was R = 42.6 mm.

The acoustic transducer operates as an emitter-receiver, the root-mean-square (RMS) of the received voltage, V, as a function of distance from the probe being the basic measurement used to determine the bed depth: being solid surfaces, both (a) the lower pipe wall and (b) the top of a settled bed of particles are strongly reflective and produce a sharp peak in V. The position of (a) is used in a low-concentration test run to calibrate the exact position of the probe by finding its position relative to the pipe walls. The resulting positional offset, a_{off}, would then be applied to all subsequent runs using this particular probe arrangement. The position of (b) is then used to measure the total bed depth, h, over time in runs where a bed is present.

The flow Reynolds number, Re_{flow}, is defined as follows:

$$\text{Re}_{flow} = \frac{U_{flow}H}{\nu},$$ [15]

where H is the fluid depth, *i.e.* the distance from the lower pipe wall or sediment bed surface if present, to the upper pipe wall. The bed and flow geometry are as described by Rice *et al.* (2015a). For time-dependent bedforms, the total bed depth can be divided into two components such that:

$$h = h_b + h_s,$$ [16]

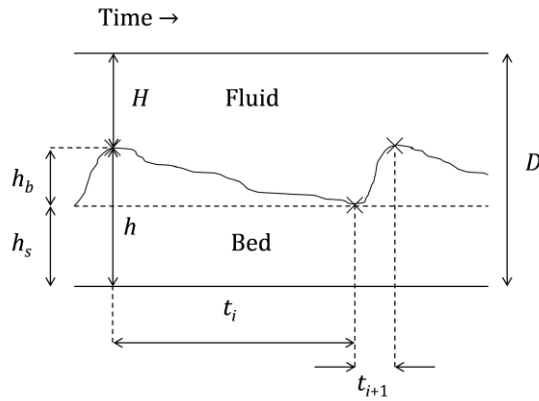where h_b is the bedform height and h_s is the depth of the settled part of the bed, as illustrated in Figure 1.

Figure 1: Time-dependent bedform geometry and evolution. H and h are fluid and bed depths, with $h = h_b + h_s$, where h_b and h_s are bedform height and settled bed depth, respectively. R and D are pipe radius and diameter; t_i is ith period between adjacent peak and trough.

3.3 Summary of experimental procedure

The experimental procedure for each set of runs was as follows:

1. A known mass of solids corresponding to the nominal volume fraction, ϕ_w, was added to the mixing tank (ϕ_w = 0.1, 0.5, 1 and 3% by volume); the mixer and pump turned on to produce a fully suspended flow throughout the flow loop.

2. The pump rate was reduced to a low value for several (5-10) minutes, in order that suspended particles settled in the test section and a flat, stationary bed of particles that did not vary over time was generated. This was then the nominal initial bed depth for the run.

3. The *UVP-DUO* (and video camera, when used) was set running, and the flow rate was set to its nominal value for the run.

To summarize, the distance to the opposite pipe wall is found using a reference run, as described in Section 3.2. In practice this meant the flow rate had to be high enough that the sediment was fully suspended and a settled bed (the top of which would act as a reflective surface itself) was not present. The settled bed thickness could then be calculated in a simple fashion.

Echo profiles (n = 500 to 5,000 samples) through a vertical cross-section of the horizontal test section were taken with a transducer operating at 4 MHz and mounted at 90 degrees to the mean flow direction. The root-mean-square of the received voltage, V, over groups of n_s = 20 samples was then calculated (*i.e.* Δt = 1.86s, sample interval = 93 ms), from a sample rate of approximately 10 Hz. Four nominal solid volume fractions were used: ϕ_w = 0.1, 0.5, 1 and 3 %,

12

as this meant a large range of initial bed depths could be generated, with mains water as the carrier fluid and plastic particles (Guyblast 40/60; see Table II) as the solid. The volumetric flow rate, Q, was varied over a range of $0.06 < Q$ (l/s) < 0.9 and the Reynolds number, Re, over a range of $1{,}800 < \text{Re} < 26{,}000$.

All runs were contrived to begin with an upper-plane (*i.e.* flat) moving bed with no time-dependent behavior, as the remit of the study was the initial behavior of time-dependent bedforms. This state corresponds to the initial value of the flow rate, Q, and bed depth, h. The latter is the first control parameter. The flow rate was then reduced to its nominal final value. This is the second control parameter. This procedure was used for consistency and because the two control parameters are thereby uniquely defined.

4   Results and discussion

4.1   Threshold for incipient particle motion

A total of four runs were identified – visually, then by inspection of acoustic measurements for verification – as being at the threshold of particle motion. Using the method of Peysson *et al.* (2009) given in the appendix, a mean value for the critical Shields number – *i.e.* that at incipient particle motion (and see Equation [12]) – of $\theta_{sc} = 0.094 \pm 0.043$ was measured, based on those four data and with the relative roughness constrained to $\varepsilon/D^* = 0.01$ in each case (Peysson *et al.*, 2009), where it is noted that $\varepsilon/D^* \sim d/D$; here ε is the roughness coefficient and D^* is a length scale (see appendix), and $d_{50}/D = 0.011$. The measured value of θ_{sc} falls in the range given by Ouriemi *et al.* (2007) of $\theta_{sc} = 0.12 \pm 0.03$, based on a large number of data from the literature, and also agrees well with the direct numerical simulations results of Kidanemariam and Uhlmann (2014) in channel flow with several particle types and flow conditions.

An estimate of the critical Shields number was also made using the method given by Soulsby (1997) – see the appendix – yielding a value of $\theta_{sc} = 0.038$, *i.e.* a significant under-prediction of the measured value given above. It is noted that the Soulsby (1997) method was employed by Edelin *et al.* (2015) and was found to accurately predict measured values in pipe flow with spherical, buoyant particles ($s = 0.910$, $d_{50} = 756\ \mu\text{m}$).

4.2   Categorization of observed bedforms

The observed bedforms are categorized into five types according to their behavior and evolution over time (or lack thereof). Three examples of bedform fields that form from initially planar beds are shown in Figure 2, Figure 3 and Figure 4. In Figure 2 ($Q = 0.498$ to 0.403 l s^{-1} at $t = 0$, $\phi_w = 0.1$ %) a ripple bed forms with a regular period, that grows to an equilibrium height,

while in Figure 3 (Q = 0.483 to 0.323 l s^{-1} at t = 0, ϕ_w = 0.5 %) it appears that a ripple-bed forms initially (with a small frequency period) which transitions to a field of dune-type bedforms with longer period.
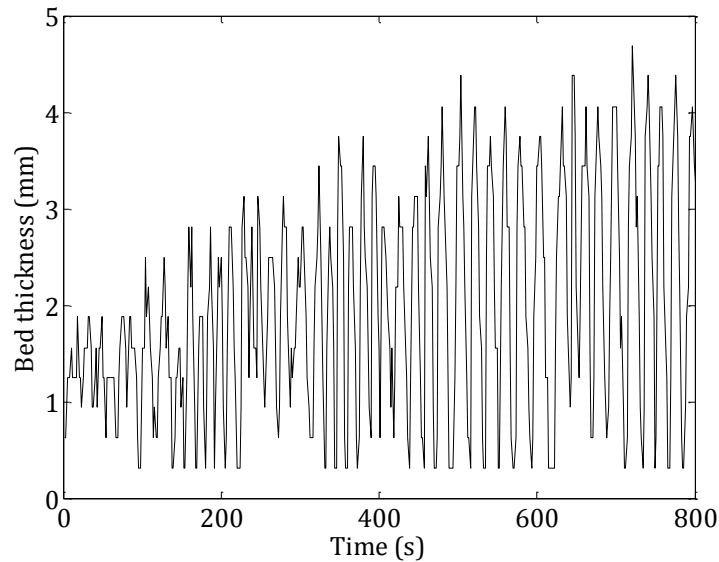

Figure 2: Bed thickness against time: shallow, regular ripples (Q = 0.498 to 0.403 l s^{-1} at t = 0, ϕ_w = 0.1 %).

The bed thickness in Figure 4 (Q = 0.383 to 0.287 l s^{-1} at t = 0, ϕ_w = 1 %) exhibits more complex behavior, varying strongly and cyclically, and the ripple/dune field is not at equilibrium at the end of the run (more than 30 minutes). The bed thickness exhibits bi-periodic behavior that suggests that at least two competing modes are present, and the bedforms quite abruptly transition from ripples to dunes and back again. Similar periodic behavior has been observed by Edelin *et al.* (2015) in studies of ripple formation with neutrally buoyant particles in pipe flow, although in their case, two distinct ripple formations were observed with differing wavelengths and similar amplitudes, unlike in the present study.
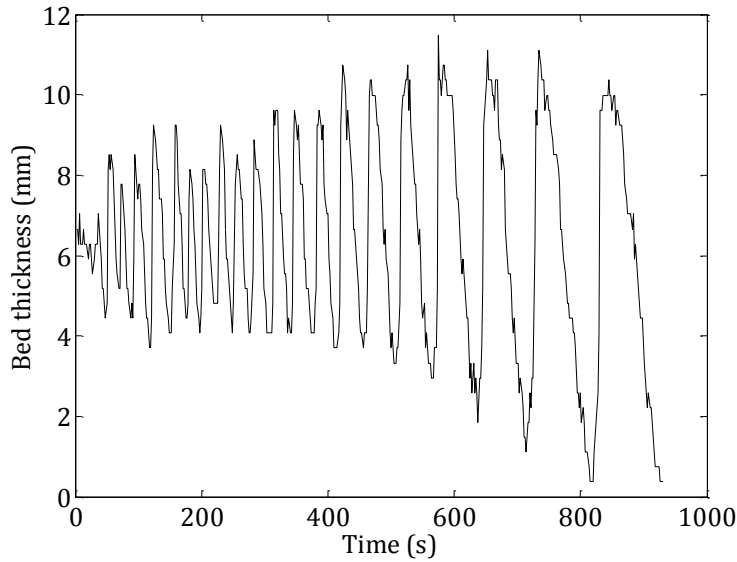
14

Figure 3: Bed thickness against time: transitioning ripple-to-dune formation with increasing period (Q = 0.483 to 0.323 l s^{-1} at t = 0, ϕ_w = 0.5 %).
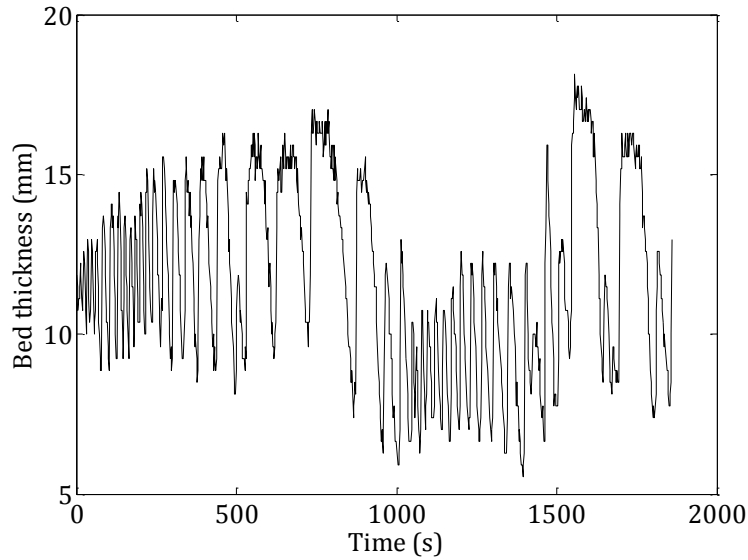

Figure 4: Bed thickness against time: unstable and cyclic ripple-to-dune formation (Q = 0.383 to 0.287 l s^{-1} at t = 0, ϕ_w = 1 %).

For the purpose of consolidation and summary, a list of observed bedform types is given in Table III, categorized broadly and in order of decreasing flow rate. It is important to note that ripples of increasing period may, in fact, be of the unstable/cyclic type, as discussed in more detail below. However, while there are similarities between them, the differences are significant enough based on the evidence collected for two categories to be defined, although it is not known how universal the delineations are. For brevity, example runs are not shown for two further bedform types: upper plane beds and beds with no particle motion.

15

Table III: Categories of bed/bedform identified in this study.	
Bed/bedform type	Description
1 Upper plane bed	Planar (*i.e.* flat) bed: depth does not vary over time, once equilibrated. Transitional between time-varying bedforms and heterogeneous suspension.
2 Bedforms of regular period	Ripples of time-independent period: period of ripples remains constant; depth may increase with time. Example: Figure 2.
3 Bedforms of increasing period	Ripples of time-dependent period which transition to dune formations; depth may also increase with time. Example: Figure 3.
4 Bedforms with unstable/cyclic period	Ripples and dunes of complex time-dependent periodicity, suggesting at least two competing modes. Example: Figure 4.
5 Bed with no particle motion	No particle motion occurs on surface of bed; determined visually. (Plots of such runs show a flat line, so no example is provided.)

In order to complement the acoustic data and verify the identification of bedform categories given above, a concatenated video from a single experiment (1200 seconds initial h/D = 0.278, Q = 0.191 l s^{-1}, Re$_{flow}$ = 5341) was analyzed, the bed surface identified and the wavelength, λ_b, and bedform celerity, c_b (*i.e.* rate of progradation), computed, where the wavelength and celerity are related as follows:

$$c_b = f_b \lambda_b. \qquad [17]$$

Here f_b is the bedform frequency and was calculated as the reciprocal of the bedform period at a fixed measurement point in the video images. The videos were recorded contiguously and were concatenated into a single dataset, as shown in Figure 5. Ripples of regular period were observed, and mean values of the ripple frequency, wavelength and celerity of f_b = 0.010 ± 0.003 s^{-1}, λ_b = 75.2 ± 10.4 mm and c_b = 0.731 ± 0.079 mm/s, respectively, were recorded, of which the wavelength compares well with the value predicted for the initial stage of bedform development – given in Equation [13] herein, based on Coleman and Eling (2000) and Coleman *et al.* (2003), *i.e.* λ_b = 99 mm. The deviation in the apparent bed depth, δ_r, due to refraction in the pipe wall was calculated as a function of bed depth, h, but was not incorporated into the results shown in Figure 5(c) because (a) δ_r was found to be small (0.2 ≲ δ_r (mm) ≲ 1 mm over the range 8 ≲ h (mm) ≲ 18), and (b) this optical distortion does not affect the measurements of bedform frequency, wavelength and celerity, which are all calculated from extrema in the time series. Details of the calculation of δ_r are given in the Supplementary Material. It is also noted that optical distortion due to the lens itself was no more than 0.1% (DxO Labs).
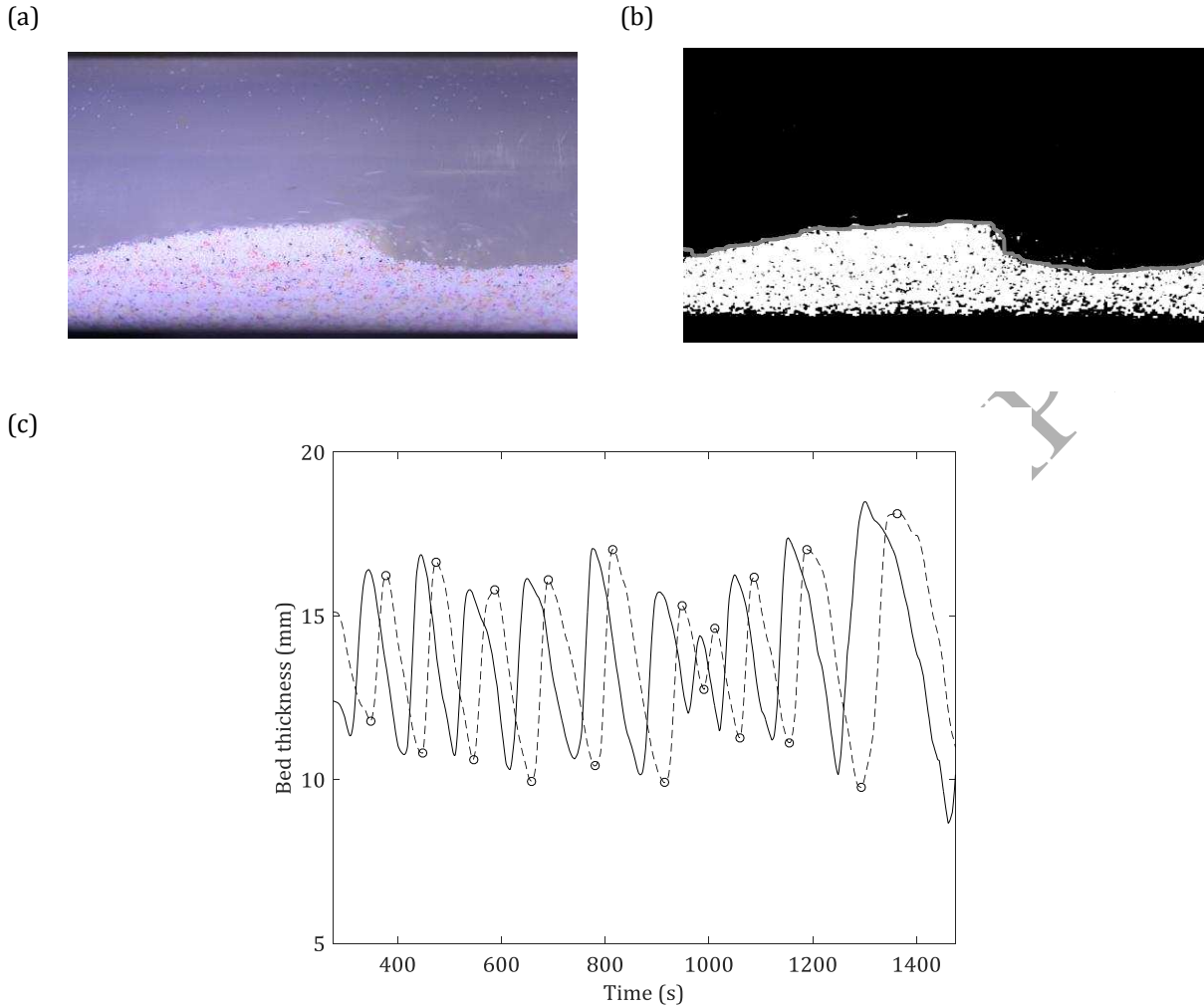
(a)

(b)

(c)

Figure 5: Video image analysis results (Q = 0.191 l s^{-1}, ϕ_w = 0.5 %). (a) Frame from video, example, image dimensions: 1920 by 1080 pixels, 75.7 by 42.6 mm; (b) binary (black and white) image of same frame as in (a), solid gray line indicates bed surface (flow from left to right); and (c) bed thickness, extracted from video, at two horizontal positions (solid and dashed lines; solid upstream) separated by 27.6 mm, times corresponding to peaks and troughs (circles) also indicated for downstream position.

Of the bedform categories defined above, regular ripples correspond to a shorter-wavelength mode, which grows comparatively slowly (Figure 2). The origin of the longer-wavelength mode (dunes) appears to be through one of two routes; via a progressive transition from growing ripples (Figure 3; and left hand-side of Figure 4), akin to the ideas of pattern coarsening of ripples (Charru *et al.*, 2013; Fourrière *et al.*, 2010), or from a marked and rapid change in mode (right hand-side of Figure 4) perhaps suggestive of an underlying instability. In the case of a progressive transition this process occurs quite rapidly (<500-1000 seconds) perhaps reflecting the faster formation of bedforms in closed conduits than in open-channel flows (Coleman *et al.*, 2003). The mechanism responsible for the unstable behavior observed in Figure 4 at $t \approx 1{,}000$ s

17

is not clear and has not been observed before, but it is suggested that it is a manifestation of competition between crest erosion at the highest parts of the bedforms, and modification of the flow area by bedforms: as bedform thickness increases, the effective flow area is reduced, and so the mean flow velocity and pressure drop increase, which acts to increase erosion and reduce bed thickness.

Additionally, hysteresis was observed under a range of experimental conditions, of which Figure 6 (Q = 0.483 to 0.323 to 0.483 l s^{-1} at t = 0, $|\Delta Q|$ = 0.160 l s^{-1}, ϕ_w = 0.5 %) and Figure 7 (Q = 0.342 to 0.277 to 0.342 l s^{-1} at t = 0, $|\Delta Q|$ = 0.065 l s^{-1}, ϕ_w = 3 %) are two examples. In both figures, upon reduction of the flow rate (first frame of each figure) the initially planar beds develop an instability in the form of ripples of increasing period transitioning to dunes (similar to Figure 3). Upon increase of the flow rate again (second frame) the ripples are washed out and the bed tends towards a planar configuration: in Figure 7 this occurs monotonically, whereas in Figure 6 periodicity remains on the bed surface. This periodicity is transient and is likely to represent simple erosion of existing bed formations, the result of a competition between erosion and sedimentation. The stabilizing effect that ultimately produces an upper plane bed from ripples and dunes is thought to arise from increased sediment transport and therefore increased "crest erosion" (Charru, 2006). This mechanism has the effect of dragging particles over the crests of bedforms – where the local fluid velocity is enhanced due to narrowing of the effective flow area – and into troughs (Andreotti and Claudin, 2013).
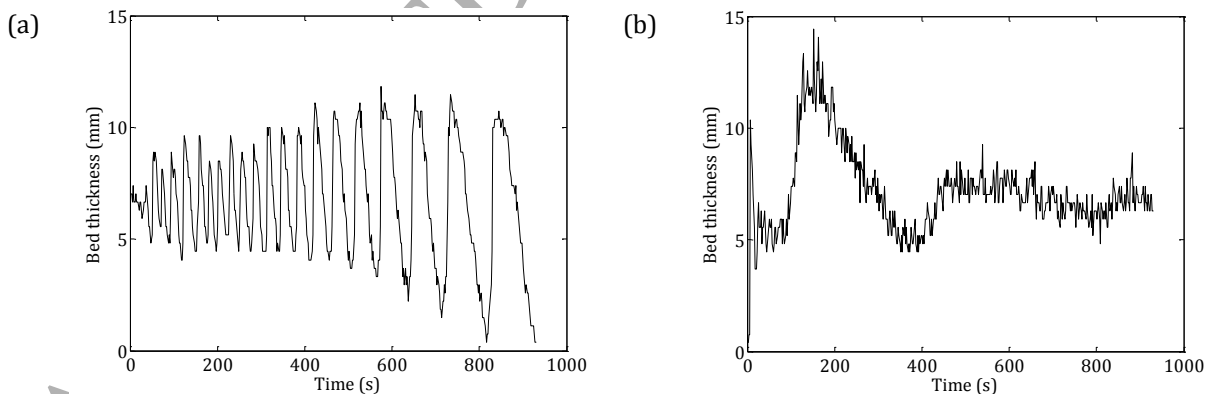

Figure 6: Bed thickness against time from acoustic data, showing hysteresis behavior, (a) Q = 0.483 to 0.323 l s^{-1} at t = 0, (b) Q = 0.323 to 0.483 l s^{-1} at t = 0 ($|\Delta Q|$ = 0.160 l s^{-1}, ϕ_w = 0.5 %). Runs were performed concurrently.
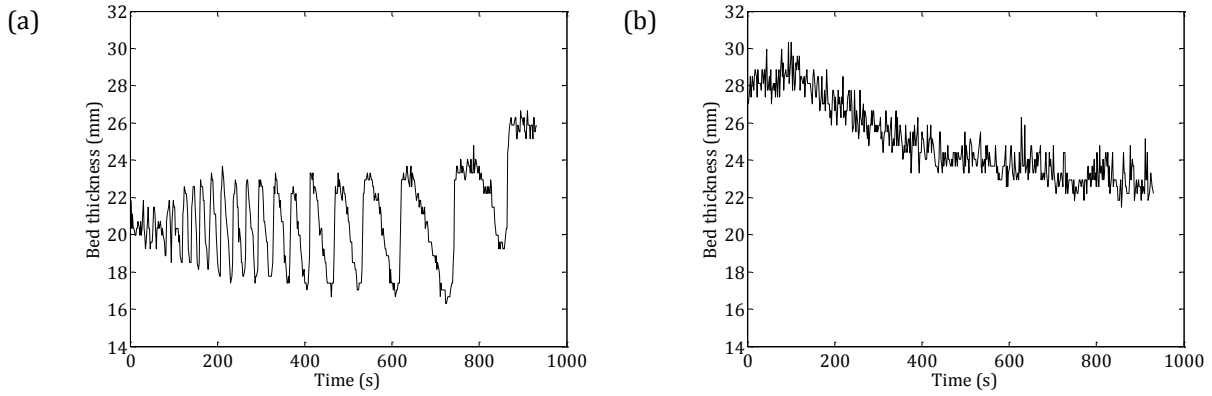
Figure 7: Bed thickness against time from acoustic data, showing hysteresis behavior, (a) Q = 0.342 to 0.277 l s^{-1} at t = 0, (b) Q = 0.277 to 0.342 l s^{-1} at t = 0 (|ΔQ| = 0.065 l s^{-1}, ϕ_w = 3 %). Runs were *not* performed concurrently.

4.3 Evolution and scaling of height and axial symmetry of time-dependent bedforms

The evolution of the height and axial symmetry of the three types of time-dependent bedforms identified in Section 4.2 (*i.e.* regular, increasing and cyclic) was investigated, with reference to a range of scalings from the literature described in Section 2. The three example runs are the same as those used in Section 4.2, the details of which are summarized in Table IV, and were chosen as being representative of their bedform type; h_b and f_b are the bedform height (see Figure 1) and bedform asymmetry factor (see Equation [18]), respectively.

Table IV: Summary of example runs to illustrate bedform evolution.		
Type	Flow rate, Q (l s^{-1})	Nominal conc., ϕ_w
Regular	0.498 to 0.402	0.1
Increasing (ripples to dunes)	0.483 to 0.323	0.5
Unstable/cyclic	0.383 to 0.287	1

A MATLAB algorithm was used to smooth the bed depth data with respect to time and then identify the local minima and maxima that correspond to the peaks and troughs of each bedform. The smoothing was necessary to eliminate scatter of the order of a few seconds (*i.e.* tens of samples), but was not found to affect the position or amplitude of peaks and troughs.

The results of the algorithm are shown for bedforms of increasing period in Figure 8, from which it is clear that the algorithm efficiently identifies the peaks – which are signified by circles – of simple regular bedforms and bedforms of increasing period.
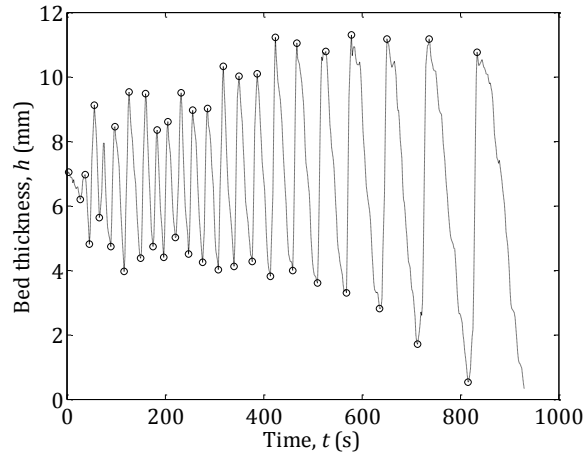
19

Figure 8: Total bed thickness, h, against time for case of bedform field of increasing period, with ripple-to-dune transition (Q = 0.483 to 0.323 l s^{-1} at t = 0, ϕ_w = 0.5 %). Circles indicate local minima and maxima (*i.e.* peaks and troughs).

The evolution and scaling of bedform height, h_b, with respect to time was investigated, using the digitized profiles. Ouriemi *et al.* (2009) found that the relative height (h_b/H) of different bedform types (specifically, "vortex" and "small dunes") were very well delineated when plotted against a dimensionless measure of time ($U_{ave}t/D$). Furthermore, several expressions are available in the sedimentology literature for the equilibrium dimensions, h_b/H, of bedforms, as given in Section 2 (García, 2008; Julien and Klaassen, 1995; Ouriemi *et al.*, 2009; van Rijn, 1984a, c). The calculated bedform depths for each bedform type in those expressions were compared, at which point it should be noted that U_{flow} and the initial value of H were used when calculating predictions of h_b/H – and therefore C', U_*' and T – according to Equations [4], [5] and [6]. The predictions are overlaid on plots of the data as horizontal lines in frame (b) of each of the three figures below (*i.e.* Figure 9, Figure 10 and Figure 11). It is also important to note that the expressions against which the results are to be compared (specifically Equations [4], [5] and [6]) are strictly for predicting *equilibrium bedform dimensions*, whereas the bedforms in this study were not thought to be at equilibrium. Therefore, while there is a significant question as to the validity of these expressions in the present case, the purpose of making the comparison was initially to confirm that the observed bedforms were, indeed, not at equilibrium. Additionally, it allowed a qualitative judgement as to which expression for equilibrium dimensions was closest to the observed bedforms, had the experimental runs been longer.

The evolution of h_b/H against t, is shown in Figure 9, Figure 10 and Figure 11, respectively, for each of the three bedform types considered above. The first clear observation to be made is that the bedform height is significantly smaller, with less scatter (with the exception of a small anomaly around t = 1,000 s), in the case of regular ripples (Figure 9) and appears to be at

20

equilibrium by t = 500 s. The observed logarithmic increase in ripple size over time is similar to that commonly seen in channel flows (Malarkey *et al.*, 2015) and is of a similar order to ripple formations found in floating beds of neutrally buoyant particles in closed-pipe flow (Edelin *et al.*, 2015).

Importantly, the equilibrium profiles satisfy the definition of ripples, by being substantially under the h_b/H ratio for dune transition predicted by Julien and Klaassen (1995) and van Rijn (1984a), as given in Equations [5] and [6]; h_b/H also remains below the 1/6 value of García's (2008) dune predictor in Equation [4], although as noted earlier this expression does not distinguish between dunes and ripples. It is thought that these definitions, derived for open-channel flow, are however not valid for closed conduits such as pipes. Conceptually, the most important difference is the lack of a free surface: in a closed-conduit flow, the no-slip condition at the upper wall means the local flow velocity near the bed surface – and therefore the shear stress and, if the relevant conditions are met, the sediment transport rate – is likely to be larger than in an open-conduit flow with properties (*i.e.* cross-sectional area and bulk flow rate) that are otherwise the same. In this way, the discrepancy between the expressions of García (2008), Julien and Klaassen (1995) and van Rijn (1984a) and the bedform dimensions measured in this study in a closed conduit can be understood: the velocity and shear stress fields generate different bedform behavior than in open conduits.

Figure 9: Scaling and evolution of bedform height, h_b, relative to fluid height, H, against time, t, for case of ripple bedform field of regular period (Q = 0.498 to 0.402 l s^{-1} at t = 0, ϕ_w = 0.1 %).

Inspection of Figure 10 (bedforms of increasing period, showing a ripple-to-dune transition) and Figure 11 (unstable/cyclic bedform fields alternating over time between ripples and dunes) reveals very similar initial behavior – a monotonic increase in bedform height, albeit with some

21

scatter, for $0 < t$ (s) < 500. At that point, however, the behavior of the two bedform types diverges: in the first (Figure 10), h_b continues to rise with a secondary phase, from t > 500, and does not reach an equilibrium height within the timescale of the experiment. In Figure 15, the h_b ratio becomes extremely unstable, with phases that appear at a ratio less than 0.2 and more than 0.3, although with significant scatter. While quantitative distinctions between these oscillating cases are difficult to make, there appears to be value in comparison to the dune transition correlations of Julien and Klaassen (1995) and van Rijn (1984a). h_b/H ratios in both Figure 10 and Figure 11 approach that for dune transitions as described by van Rijn (1984a), although the ratios are significantly below that of Julien and Klaassen (1995). The likely reason for the closer correlation to the van Rijn (1984a) relationship is that it contains a larger number of flow-specific parameters that more accurately account for pipe flow but which are absent from the García (2008) and Julien and Klaassen (1995) expressions.
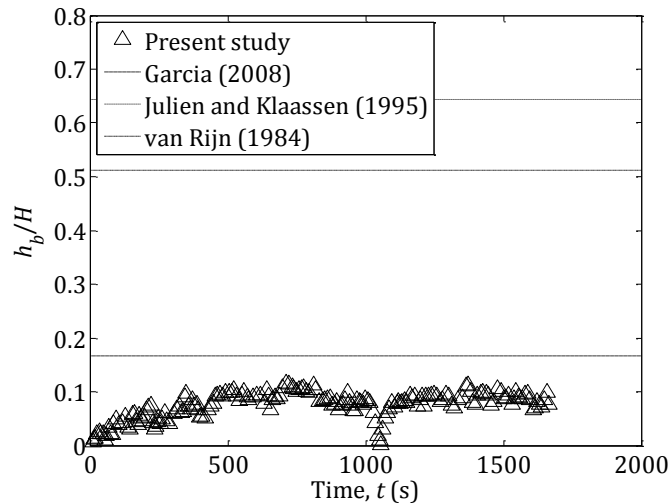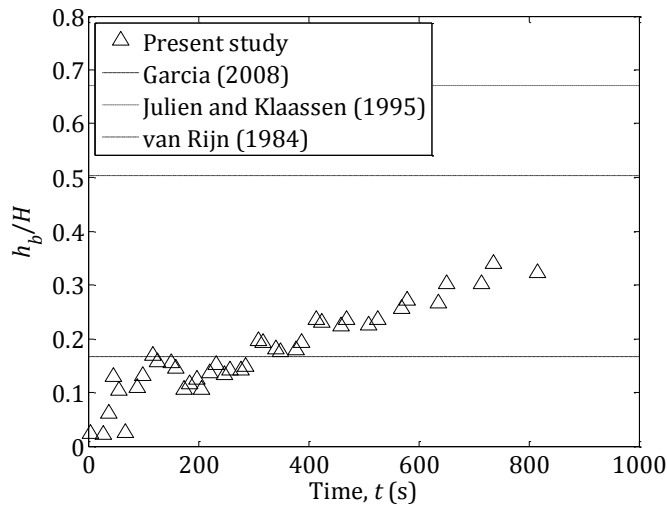

Figure 10: Scaling and evolution of bedform height, h_b, relative to fluid height, H, against time, t, for case of bedform field of increasing period (Q = 0.483 to 0.323 l s^{-1} at t = 0, ϕ_w = 0.5 %).
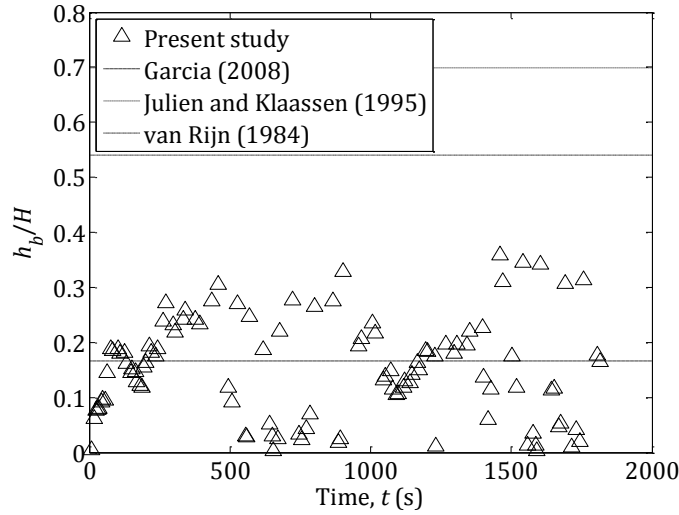
Figure 11: Scaling and evolution of bedform height, h_b, relative fluid height, H, against time, t, for case of unstable/cyclic bedform field alternating between ripples and dunes (Q = 0.383 to 0.287 l s^{-1} at t = 0, ϕ_w = 1 %).

To provide further evidence for the ripple-to-dune transition, the axial symmetry of the three time-dependent types of bedforms was investigated, and was quantified by the bedform asymmetry factor, f_b, defined as the ratio of the periods between adjacent minima and maxima in the bed depth, as illustrated by t_i and t_{i+1} in Figure 1 and shown below:

$$f_b = \frac{t_1}{t_2}. \hspace{4cm} [18]$$

Here, t_1 and t_2 are the larger and smaller of t_i and t_{i+1}, respectively (which are illustrated in Figure 1). It is clear, then, that f_b was contrived to be the ratio of the larger to the smaller of adjacent periods, so that $f_b \geq 1$, in order to allow a clearer illustration of the development of asymmetry with time, where it would be expected that formation of dunes would correlate to an increase in f_b. Celerity and wavelength could not be measured with the acoustic system, as a single probe was used to measure bed depth. However, f_b, although a ratio of periods, is intended to be a proxy for the ratio of wavelengths of the same bedforms, which is reasonable if it assumed that the change in celerity between adjacent bedforms is small.

Plots of the bedform asymmetry factor, f_b, are shown for the three example runs (see Table IV) in Figure 12(a) for regular ripples, ripples with increasing period and unstable/cyclic bedform fields. In the case of regular ripples, f_b remains small (f_b < 2 for the vast majority of bedforms) and shows no significant trend over time, and comparison of Figure 12(a) with Figure 9 (h_b/H against time) confirms that the bedforms remain stable, quite axially symmetrical and of small amplitude relative to the pipe diameter and fluid depth. The trends for increasing-period ripples

23

and unstable/cyclic bedforms are: an increase in asymmetry over the first few hundred seconds, followed by significant scatter; and much higher values of f_b compared to the first case (regular ripples). When the evolution of bedform height, h_b (Figure 10 and Figure 11) is compared with that of bedform asymmetry, there is a broad correlation that deeper bedforms are more axially asymmetrical, as would be expected for dune-type bedforms, with unstable/cyclic bedform fields becoming most asymmetrical. The bedform types are summarized schematically in Figure 12(b).

(a)

(b)

Figure 12: (a) Bedform asymmetry factor, f_b, against time for regular ripples (solid black line; Q = 0.498 to 0.402 l s^{-1} at t = 0, ϕ_w = 0.1 %), ripples with increasing period (dashed black line; Q = 0.483 to 0.323 l s^{-1} at t = 0, ϕ_w = 0.5 %) and unstable/cyclic bedforms (solid gray line; Q = 0.383 to 0.287 l s^{-1} at t = 0, ϕ_w = 1 %); (b) schematic summary of bedform types.

4.4 Influence of solids volume fraction and particle sphericity and roundness

In the first instance, the main influence of the solids volume fraction, ϕ_w – which is that of the whole system, as was the case in the study of Edelin *et al.* (2015) – is on the range of achievable initial bed depths. Specifically, higher volume fractions allowed for thicker beds to form, as the

test section of the flow loop acted as a sink in which particles could readily settle. The values of h/D corresponding to ϕ_w = 0.1, 0.5, 1 and 3% by volume are approximately: $0 < h/D < 0.08$, $0.08 < h/D < 0.18$, $0.18 < h/D < 0.4$ and $h/D > 0.4$, respectively.

Gore and Crowe (1989, 1991) found that turbulence intensity in multiphase pipe and jet flows was either attenuated or enhanced relative to equivalent single-phase (*i.e.* unladen) flow according to the value of d/l_e, where d is the particle diameter and l_e is the length scale of the most energetic turbulent eddies such that $l_e \approx 0.1\ D$ (Hinze, 1959). Above and below $d/l_e \approx 0.1$, turbulence intensity is enhanced or attenuated, respectively. In the experiments presented here, d/l_e = 0.110, and so the modulation effect is likely to be negligible.

Once a bed had formed in the flow apparatus, the ambient volume fraction appeared to be very low, as it was depleted by the existing bed, as is clear from Figure 13 (same run as in Figure 5: see also associated text), and from visual inspection during the runs. The similarity with images of bedforms in motion presented by Gao (2008) and others (Edelin *et al.*, 2015; McLean *et al.*, 1994; Raudkivi, 1963) is noted. Although in the present experiments the turbulence modulation effect was likely negligible, in general it would be expected to increase with solids concentration and affect the deposition behavior.

The particle sphericity and roundness were measured in order to quantify their effect on settling velocity as it pertains to incipient motion and bedform behavior. The expression given by Dietrich (1982) for settling velocity – see the appendix – was evaluated using measured values of the Corey shape factor, F_s (a measure of sphericity) and the Powers roundness factor, P, measured with a Retsch *Camsizer XT* optical shape analyzer. The calculated settling velocities were then compared to those for equivalent particles of perfect smoothness and sphericity to quantify the effects of those properties. The results are summarized below.
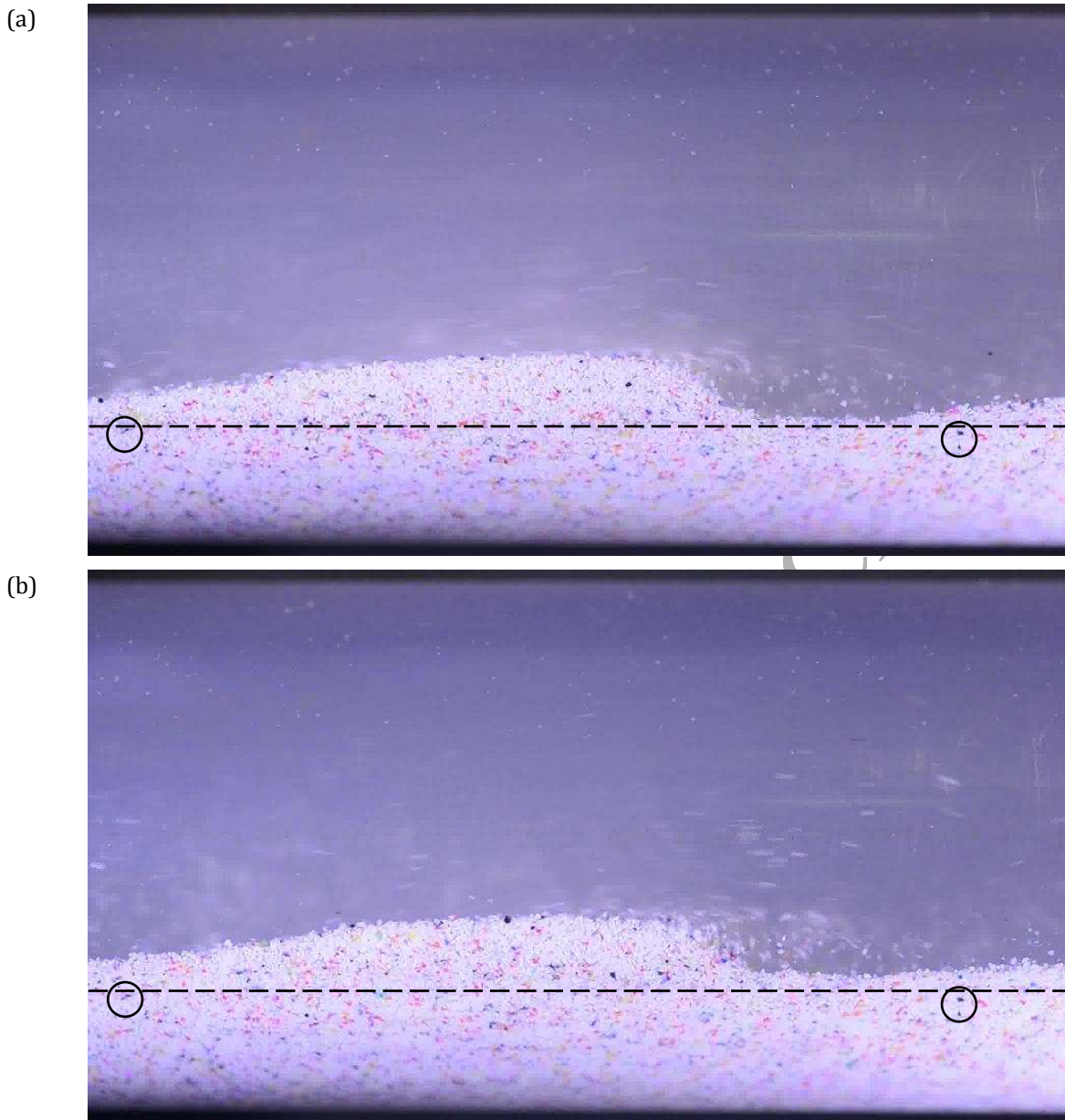
25

Figure 13: Images of flow over regular ripple bed (Q = 0.191 l s^{-1}, ϕ_w = 0.5 %; 1920 by 1080 pixels, 75.7 by 42.6 mm). Dashed lines represent boundary between stationary and moving parts of bed, from inspection of detail in images. Images (a) and (b) from same run, separated in time by $\Delta t \approx 3.5$ minutes and showing different ripples. Circled areas show examples of common bed features in stationary part of bed.

1. The median particle size (*i.e.* d_{50}) measured with the optical instrument and assumed to be that of a circle of equivalent projected area, was 442 μm, very close to the value of 468 μm measured with the *Mastersizer* laser-diffraction instrument (see Table II);

2. The Corey shape factor was measured to be F_s = 0.842 (where a value of 0 corresponds to a rod and 1 to a sphere; Corey, 1949; Dietrich, 1982) with a corresponding reduction in dimensionless settling velocity, w^*, to 0.79 of that for an equivalent spherical particle (*i.e.* with F_s = 1);

3. The Powers roundness factor was measured to be P = 2.49, corresponding to a "sub-

angular" shape (on a scale from 0: "very angular" to 6: "well rounded"; Powers, 1953; Syvitski, 2007) with a corresponding reduction in dimensionless settling velocity, $w*$, to 0.91 of that for an equivalent well-rounded particle (*i.e.* with $P = 6$).

4. The effect of both Corey shape factor and Powers roundness factor was to reduce the settling velocity, $w*$, to 0.77 of that for an equivalent spherical, well rounded particle (*i.e.* with $F_s = 1$ and $P = 6$), where it is noted that the effects of F_s and P given above individually do not combine in a simple way.

So, the shape and roundness of the particles strongly affect the settling behavior of the particles such that the particles are more readily suspended, and bedforms are thereby expected to be eroded and migrate more quickly than they would with equivalent spherical particles. Critically, the settling velocity is intimately involved in resuspension and incipient particle motion, which proceeds when the bed shear velocity becomes comparable to the settling velocity (Hinze, 1959; van Rijn, 1984b). So, to first order, particle shape might be expected to reduce the flow rate necessary for incipient particle motion, which is consistent with the value of the critical Shields number calculated here being lower than that predicted by Ouriemi *et al.* (2007), as described earlier.

Lastly, it is noted that Clark *et al.* (2015) found that the threshold for particle motion has a strongly hysteretic character: that is, the threshold differs depending on whether the flow rate is decreased until the particles cease to move, or if the flow is gradually increased until particles on the surface of an initially stationary bed begin to move. It is clear that this mechanism, along with the others described above, contributes to the complexity of bedform behavior, that complexity being greater in the case of angular, non-spherical particles.

4.5   *Phase diagrams of bedforms in closed pipe flow*

A phase diagram of bedform types – as categorized in Table III – is presented in Figure 14 in terms of the bulk Reynolds number, Re_{pipe} (Equation [1]), against $Ga(H/d)^2$ (see Equation [2] for the Galilei number, Ga), where H and d are the fluid depth and particle diameter, respectively. It is noted that Ga is constant for a given particle species and so the quantity that varies in Figure 14 is the ratio H/d. These variables are as used by Ouriemi *et al.* (2009) with silica particles. It should be noted that H is the initial value before the bed surface is perturbed by a change in flow rate. These quantities were chosen because they have a common interpretation in all the runs and could be evaluated in a consistent way. It should also be noted that the three-dimensional "sinuous dunes" observed by Ouriemi *et al.* (2009, 2010) were not observed in the present study: all bedforms were two-dimensional (by visual inspection). Data from a total of 58

runs at several nominal concentrations ($0.1\ \% < \phi_w < 3\ \%$) are presented and a summary table of all the runs is given in the Supplementary Material.
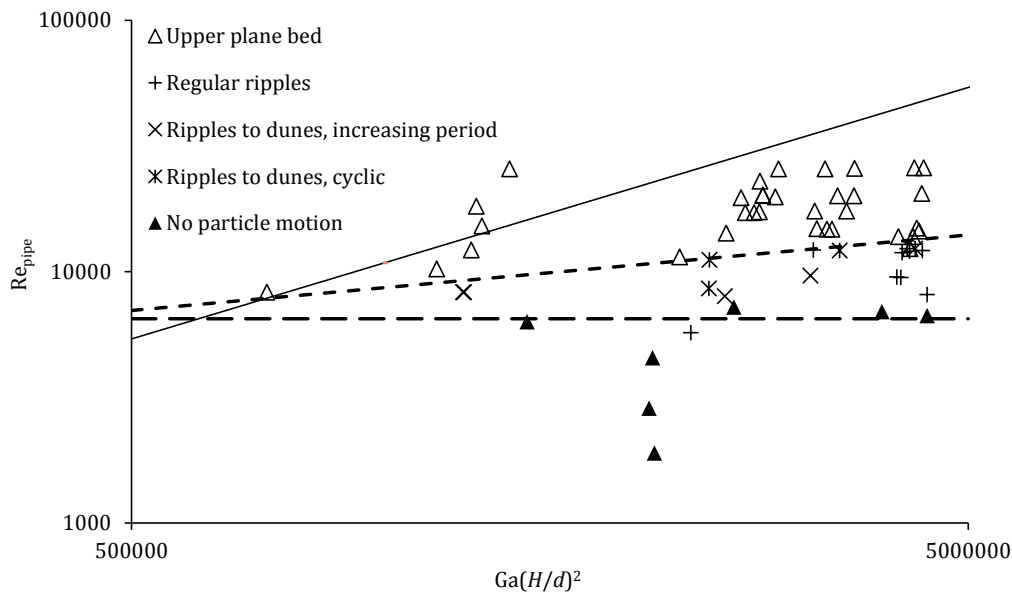

Figure 14: Phase diagram of bedforms in pipe flow according to bulk Reynolds number, Re_{pipe} against $Ga(H/d)^2$. Unfilled triangles: upper plane bed; pluses: regular ripples; crosses: unstable ripple-to-dune cycles; stars: ripples that transition with increasing period to dunes; filled triangles: no particle motion. Dashed lines indicate transitions between no particle motion, time-dependent bedform fields and upper plane beds, and are fitted visually. Solid line is prediction for incipient particle motion threshold from Ouriemi *et al.* (2009).

The regions in Figure 14 corresponding to no particle motion, ripples/dunes and upper plane beds are well delineated. The three time-dependent bedform types are less well delineated, but the tentative observation can be made that regular ripples are clustered at higher values of $Ga(H/d)^2$ and increasing and unstable ripple-to-dune formations at lower values. This (a) is an inversion relative to the observations of Ouriemi *et al.* (2009), who observed "small dunes" at lower values of $Ga(H/d)^2$ and larger, "vortex dunes" at higher values; and (b) highlights that they generally occur in conditions where the flow thickness becomes an important factor, although clear delineations between the two bedform types are not immediately evident. Additionally, this behavior suggests they are transitional between ripples and upper plane beds. There is a clear dependence of bedform type on Reynolds number, while it appears that both ripples and dunes occur in a relatively small region around $Re_{pipe} = 10{,}000$ (and thus all within a turbulent flow field).

To reiterate, inspection of the bulk Reynolds number, Re_{pipe}, in Figure 14 demonstrates that the

flow was turbulent in all runs except for two, in both of which no particle motion was observed. In particular, these two runs had Re_{flow} = 1780 and 2680; the flow was therefore laminar and transitional/turbulent, respectively, assuming the transition in pipe flow occurs in the region of $Re_{flow} \approx$ 2300-2500 (Edelin *et al.*, 2015; Ouriemi *et al.*, 2009). However, the flow rates for the two laminar runs were below that for incipient particle motion.

A number of other observations and conclusions can be drawn from Figure 14, which is plotted with the same variables as the phase diagram of Ouriemi *et al.* (2009). First, the threshold for particle motion ($Re_{pipe} \approx$ 6,500) does not vary with Ga(H/d)^2. Second, the threshold between unstable bedforms and upper plane beds appears to increase with Re_{pipe}. Third, the same threshold vanishes at low flow Ga(H/d)^2, although this observation is tentative as it is based on rather few data. Fourth, and most importantly, the observed thresholds do not appear to closely match those given by Ouriemi *et al.* (2009), although it is difficult to gauge the closeness of the match as the results presented here fall into a small area in the upper limits of the parameter space investigated by Ouriemi *et al.* (2009). The threshold for incipient particle motion according to the expression given by Ouriemi *et al.* (2009) was calculated, namely Re_{pipe} = $(2\theta_{sc}/3\beta\pi)$Ga(H/d)^2 = 0.0108 Ga(H/d)^2, where β is a fitting constant found by Ouriemi *et al.* (2007) to be β = 1.85 and θ_{sc} = 0.094 as measured here, but the expression does not correctly predict the observed threshold for incipient particle motion, as is clear from Figure 14. It is also noted that the instability threshold predicted by Ouriemi *et al.* (2009), namely Re_{pipe} = $140\phi_m/3\beta\pi\theta_{sc}$ = 43.9, where ϕ_m is the maximum packing fraction in the bed, with ϕ_m = 0.514 (Rice *et al.*, 2015a), under-predicts the Reynolds number at which ripples are first observed in the present study by several orders of magnitude – and, in fact, falls below the threshold for incipient particle motion – and is therefore not included in Figure 14.

These differences are not surprising because: (a) the Ouriemi *et al.* (2009) model assumes viscous flow and their experiments were performed under different conditions, whereas the majority of runs were turbulent in the present study; (b) a particle flux was maintained throughout each run in the present study, whereas it was not in the Ouriemi *et al.* (2009) study; (c) all the bedforms observed in this study were two-dimensional, unlike the three-dimensional sinuous dunes of Ouriemi *et al.* (2009); and (d) Ouriemi *et al.* (2009) found *lower* plane beds – *i.e.* flat beds at lower Reynolds numbers than for ripples – whereas none were observed in this study; moreover, *upper* plane beds were observed in this study, but not by Ouriemi *et al.* (2009). So, the fluid and particle dynamics are clearly different, and the parameters most likely to account for the differences between this study and that of Ouriemi *et al.* (2009) are particle shape, size, density and particle size distribution. While Ouriemi *et al.* (2009) presented some

data from large plastic particles of a similar size to the current study, most particle types investigated were much smaller. Additionally, all particles were spherical in shape, and had much narrower particle size distributions than those used here. These parameters will affect bed roughness and saltation-induced roughness, and in particular for broader distributions such as those used here, where bed armoring (see later discussion) by the larger particles can occur, d_{50} may not be the optimal measure of particle size, and d_{90} or another parameter incorporating the size distribution range may be more suitable (Kleinhans *et al.*, 2017; Peakall *et al.*, 1996). Clearly, the position of the thresholds between the various bedform types are either very different, inverted or non-existent, depending on the particle and flow parameters. The last observation is that the variables used, as chosen by Ouriemi *et al.* (2009) – Re_{pipe} and $Ga(H/d)^2$ – do not appear to able to capture the universal behavior of bedforms in closed pipes, and an effort was made to improve the parameterization of the phase diagram.

When comparing data from natural and laboratory systems, and from conduits with rectangular, circular and other cross-sectional shapes, it is clear from the results presented that many time- and length scales can be used, but that not all are universal because the geometry – and therefore flow field and particle concentration profiles – differ. For example, a non-zero bed depth in pipe flow modifies the chord length at the bed surface and the shape of the flow area, whereas in rectangular channel flow it does not. This issue is discussed in more detail, with the aim of suggesting scalings that are more universal and allow more direct comparison of data from different flow geometries at low flow rates.

The most important point to note is that total bed depth, h, and pipe diameter, D, influence the flow behavior in so far as they modulate the flow area and bedform chord length. However, the ratio H/d does not appear to have a strong effect on the threshold for incipient motion, as is clear from Figure 14. The flow does not interact with the lower, stationary part of the bed, as can be seen in the two frames in Figure 13, and particle motion is confined to the body of the ripples.

Upon first consideration, then, the three quantities that will influence the behavior of the bed, and which ought to be chosen to allow comparison between various flow geometries, are (a) the fluid depth above the bed, (b) the fluid velocity at or near the bed surface, and (c) the size of the particles. However, it should be noted that in the special case of very large particles or very small flow cross-sections, the fluid depth or pipe diameter in the case of a very thin bed would be an important parameter. This is not the case in this study, in which $d_{50}/D \approx 90$.

So, some combination of (a) H, (b) U_{ave}, and (c) d_{50} may appear optimal. However, it is suggested that more physically meaningful choices can be made. In the case of (a) an equivalent fluid depth, H_{eq}, is proposed and is as illustrated in Figure 15. H_{eq} is calculated by conserving the chord length, c – *i.e.* the cross-sectional width of the bed at its surface – and the flow area, A_{flow}, between flow geometries, since these two quantities are posited as being of principal importance in terms of their influence on bedform behavior. That is,

$$ cH_{eq} = A_{flow} = \frac{Q}{U_{flow}}, \qquad\qquad [19] $$

where c and A_{flow} are calculated from the measured value of h geometrically. The choice of H_{eq} also naturally yields the second parameter, (b) U_{flow}, as the most appropriate.
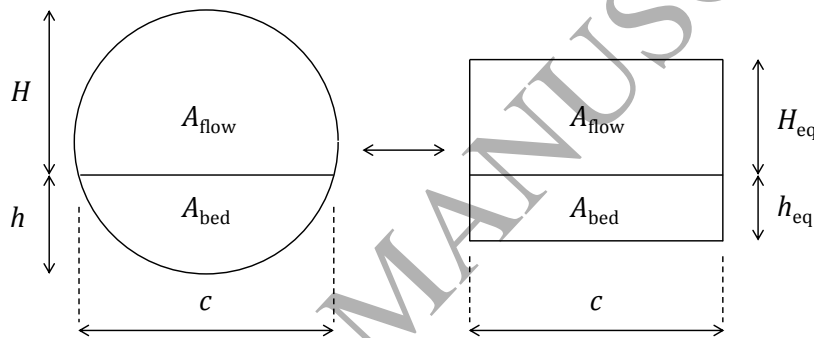

Figure 15: Illustration of a suggested universal scaling for closed-conduit flows of any cross-sectional shape.

The third choice to be made is a representative particle size at the bed surface. Although d_{50} is the most obvious choice, it may be a poor one: if the particle size distribution is wide, then the particles deposited at the surface of the bed may be significantly larger than d_{50}, since larger particles will tend to deposit more readily than smaller ones. For this reason, d_{90}, may be a better choice. Also, the size of particles at the bed surface may depend in a more complex way on the flow rate and ambient particle concentration, and the processes of armoring and overpassing, well known by sedimentologists (García, 2008; Raudkivi, 1976), may also play a role. The first is a process by which larger particles constitute the top layer of the bed, and smaller particles are thereby "armored" from the influence of fluid flow; in the second, larger particles skip over a bed of smaller particles. Indeed, in previous work on jet erosion of various mineral sediments by several of the present authors, it was found that d_{90} was a far better predictor of behavior than d_{50} for these reasons (Hunter *et al.*, 2013). It is also noted that d_{90}, rather than d_{50}, was chosen by van Rijn (1984a) as a representative particle size at the bed surface when calculating C', the particle Chézy coefficient. The resulting expressions for the

31

transport stage parameter, T, and h_b/H (Equation [6]) were found to predict equilibrium bedform dimensions more accurately than others earlier in this section, although only reasonably accurately.

So, it is suggested that choosing H_{eq}, U_{flow} and d_{90} – rather than, say, H or D, U_{ave} and d_{50} without further consideration – has the advantages of (a) capturing all the relevant scales, and (b) allowing more direct comparison between data obtained in conduits of different cross-sectional shapes. For example, in conduits with rectangular cross-sections, $H_{eq} \equiv H$. When applied to a specific case, in particular the evolution of bedform height, h_b, with time, t, as described in this section, the corresponding choice of parameters would be h_b/H_{eq} against $U_{flow}t/H_{eq}$ (rather than h_b/H against t as shown in Figure 9, Figure 10 and Figure 11). Both parameters have universal, unambiguous meanings in many flow geometries and accurately represent the physical situation in the flow, because as many important flow parameters as possible are taken in to account, and because results can readily be compared to the expressions for h_b given.

With the preceding arguments on universal scalings in mind, and with reference to a similar combination used by Ouriemi *et al.* (2009), a second phase diagram – shown in Figure 16 – was constructed based on the combination $Ga_{eq}(H_{eq}/d_{90})^2$ and Re_{eq}, which are defined as follows:

$$Re_{eq} = \frac{U_{flow}H_{eq}}{\nu}, \tag{20}$$
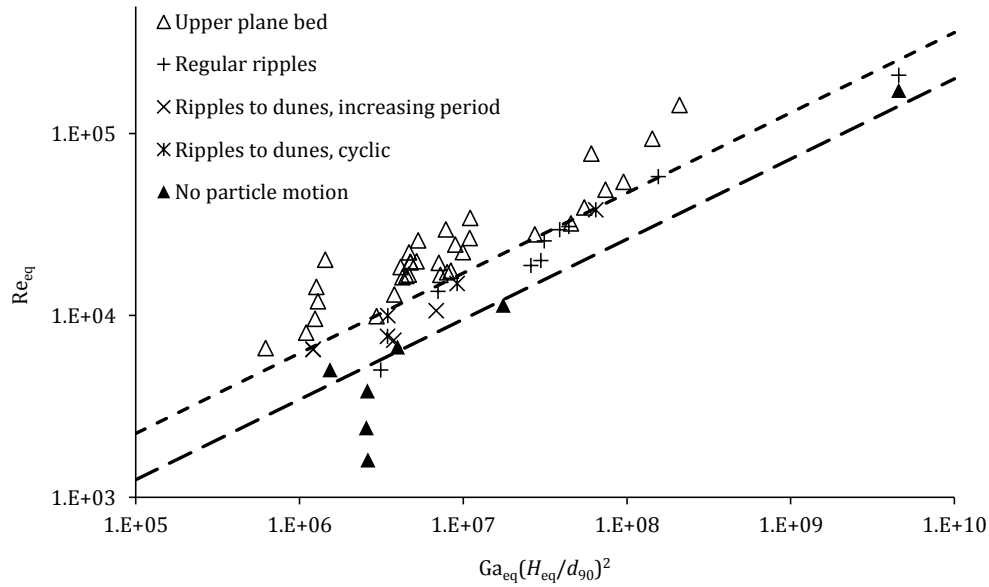
$$Ga_{eq} = \frac{d_{90}^3(s-1)g}{\nu^2}. \tag{21}$$

Figure 16: Phase diagram of bedforms in pipe flow according to equivalent Reynolds number, Re_{eq} against $\mathrm{Ga}_{eq}(H_{eq}/d_{90})^2$. Unfilled triangles: upper plane bed; pluses: regular ripples; crosses: unstable ripple-to-dune cycles; stars: ripples that transition with increasing period to dunes; filled triangles: no particle motion. Dashed lines indicate transitions between no particle motion, time-dependent bedform fields and upper plane beds, and are visually fitted.

Two important observations can be made from Figure 16. Most significantly, the small, regular ripple formations seem to be clustered at higher values of the abscissa (*i.e.* larger relative fluid depths), whereas the other two variable bedform types are clustered at smaller values. It can also be seen from Figure 16 that the initial relative fluid depth strongly influences the initial bedform type. For example, at a flow Reynolds number of $\mathrm{Re}_{eq} = 10^4$, it is conceivable that any of the five bedform types could be obtained, depending on the value of the abscissa. This dependence of bedform type on initial fluid depth is entirely absent from the literature, but has important engineering implications in terms of its possible tendency to cause blockages, plugging and flow variability generally.

So, h and D clearly have a large effect on initial bedform evolution since they determine the shape of the flow cross-section. However, the equivalent fluid depth, H_{eq}, and the generalized flow Reynolds number, Re_{eq} (which takes account of the modulated cross-sectional shape), appear to be better predictors of bedform behavior, as shown in Figure 16, *for a given initial bed depth, and once the bedform has begun to evolve*. In Figure 16, the abscissa and ordinate incorporate H_{eq} and Re_{eq} and the boundaries between the various bedform types depend on both these parameters.

It should be made clear that a major reason for presenting the first phase diagram was to

33

demonstrate that (a) it is unable to represent the range of results in the literature in a universal way, (b) a rethinking of the length scales – *e.g.* d_{90} in place of d_{50}, H_{eq} in place of H – yields a phase diagram that has more predictive power in the sense that there is a dependence on both control parameters, and (c) this rethinking allows for a direct comparison with a very large, mature body of earth sciences data which, although recorded in a range of open- and closed-conduit geometries and not just closed-pipe flow, are a manifestation of the same near-bed physics.

5   Conclusions

Measurements of time-dependent bedforms produced by the deposition of solid particles from two-phase liquid-solid flows were studied using an ultrasonic echo method in a horizontal test section of closed pipe flow loop. Results were presented for settled bed thicknesses over a range of flow rates, with hysteresis behavior in plane beds and ripples also considered. The evolution and scaling of bedform heights were then investigated. In the concluding part of the results, data gathered in a wide range of experiments were used to derive phase diagrams of bedforms in closed pipes in terms of several dimensionless numbers in which the thresholds between incipient particle motion and different bedform types were established.

Most importantly, both ripple- and dune-type bedform fields were observed under certain flow conditions, sometimes as two distinct temporally varying modes within single runs. This behavior has not been reported before, and it is thought that it may be due both to the particular particle size used in this study and to the irregular shape and roughness of the particles. Correlations for equilibrium bedform dimensions, such as those devised by García (2008), Julien and Klaassen (1995) and van Rijn (1984a), were of limited value, although the last was found to most accurately predict the height of the evolved bedforms in this study.

Several non-equilibrium phase diagrams were generated categorizing formations as stable ripples, transitioning ripple-to-dune bedform fields and cyclical, alternating ripple-and-dune formations, as well as stable upper-plane beds. It should be reiterated that this study was not intended to be of equilibrium or saturation bedform dimensions – the distinction being that the former is obtained under clear-fluid conditions whereas the latter is obtained with a constant particle flux (Edelin *et al.*, 2015) – but rather of the initial behavior beginning with flat, planar beds. This choice was driven by industrial concerns, specifically the potential problems experienced upon start-up of machinery, for example, and in the resuspension and transport of settled solids. Phase diagrams would certainly be expected to be significantly different in equilibrium and saturated conditions, as they are known to be in natural and flume/open-

channel flows. However, this study addresses only the case of initial behavior. In addition, it is noted that bedforms under equilibrium and saturation conditions in closed pipes have received very little attention, and the authors are aware of only one such study (Edelin *et al.*, 2015).

No single model, either from the sedimentology or the engineering/fluid mechanics literature, was able to fully account for the observed bedform types, in terms of a phase diagram or otherwise. It was suggested that both a full set of initial conditions – at least d_{90}, h_b, H_{eq}, t, U_{flow} and v, where H_e is an equivalent fluid depth, as illustrated in Figure 16 – as well as the magnitude and type of perturbation applied to the bed, be included in any dimensional analysis that is performed in order to derive a universal scaling for bedform dimensions. Any model must necessarily incorporate the dynamic nature of bedforms, including the hysteretic, path-dependent behavior described here, and the influence of initial and resultant bed and fluid depth and changes in flow rate, which are strongly linked. Further data would, however, be necessary in order to undertake such a task. The effect of the shape of the pipe cross-section must also be taken into account in future studies, and suitable scalings (*e.g.* U_{flow} in place of U_{ave}; H or H_e in place of D; see Section 4.5) should be chosen and justified over a range of flow geometries and particle types.

6   Acknowledgements

Appendix

Expressions for bed shear stress and Shields number

The bed shear stress, τ_b, can be written as follows:

$$\tau_b = \frac{\rho_f}{2}\left(\frac{Q}{A_{flow}}\right)^2 f(\text{Re}^*), \qquad [22]$$

where *f* is the Darcy friction factor as a function of Re*, the Reynolds number based on a length

scale, D^*, computed numerically by Peysson *et al.* (2009) and referred to as the equivalent diameter such that:

$$f = 2\left[\left(\frac{8}{\text{Re}^*}\right)^{12} + (A + B)^{-1.5}\right]^{1/12}, \qquad [23]$$

$$\text{Re}^* = \frac{D^*Q}{\nu A_{\text{flow}}}, \qquad [24]$$

$$A = \left\{-2.457 \ln\left[\left(\frac{7}{\text{Re}^*}\right)^{0.9} + 0.27 \frac{\varepsilon}{D^*}\right]\right\}^{16}, \qquad [25]$$

$$B = \left(\frac{37530}{\text{Re}^*}\right)^{16}, \qquad [26]$$

where ε is the roughness length. D^* is the diameter of an equivalent pipe having the same shear stress at the wall as at the bed surface in a flow with a bed depth of h/D; values of D^* as a function of h/D are given by Peysson *et al.* (2009). The Shields number can then be calculated from the bed shear stress, τ_b, and other known flow variables *via* Equation [12].

Alternatively, the critical Shields number, θ_{sc}, *i.e.* that at the threshold of particle motion, can be estimated using a commonly cited expression, as follows (Edelin *et al.*, 2015; Soulsby, 1997):

$$\theta_{sc} = \frac{0.3}{1 + 1.2d^*} + 0.055\left(1 - e^{-0.02d^*}\right), \qquad [27]$$

where d^* is the dimensionless particle size as defined in Equation [10].

Expressions for sphericity, roundness and settling velocity

Based on several hundred data, Dietrich (1982) derived an empirical expression for a dimensionless settling velocity, w^*, that depends on d_s, the diameter of a sphere of equivalent volume, F_s, the Corey shape factor that accounts for sphericity (with low values close to zero corresponding to highly elongated ellipsoids and a value of unity to a sphere) and the Powers roundness factor, P, which ranges from 0 ("very angular") to 6 ("well rounded") (Syvitski, 2007) and has traditionally been assessed visually to a precision of ±0.5, and

36

$$F_s = \frac{c}{\sqrt{ab}}, \tag{28}$$

where a, b and c are the longest, intermediate and shortest axes of the particle. The expression for w is as follows:

$$w^* = R_3 10^{R_1 + R_2} = \frac{w^3}{gv(s-1)}, \tag{29}$$

where w^* is the settling velocity and R_1, R_2 and R_3 are as follows:

$$R_1 = -3.76715 + 1.92944(\log d_w) - 0.09815(\log d_w)^2 \\ - 0.00575(\log d_w)^3 + 0.00056(\log d_w)^4, \tag{30}$$

$$R_2 = \left[\log\left(1 - \frac{1 - F_s}{0.85}\right) - (1 - F_s)^{2.3}\tanh(\log d_w - 4.6)\right] \\ + 0.3(0.5 - F_s)(1 - F_s)^2(\log d_w - 4.6), \tag{31}$$

$$R_3 = \left[0.65 - \left(\frac{F_s}{2.83}\tanh(\log d_w - 4.6)\right)\right]^{\{1+(3.5-P)/2.5\}}. \tag{32}$$

Here d_w is a dimensionless particle diameter based on d_s, the diameter of a sphere of equivalent volume, such that:

$$d_w = d_s^3 \frac{g(s-1)}{v^2}. \tag{33}$$

In practice, the Retsch *Camsizer XT* was used to measure d_s, Fs and P indirectly, using the analogs described in Table V below, and it was assumed that (a) $d_s = x_{\text{area}}$, (b) $F_s = F_w$ and (c) $P = 6P_k$, since $0 < P_k < 1$ and $0 < P < 6$. This method is presented as a powerful tool for quantitative assessment of the effect of particle sphericity and roundness on settling and resuspension.

Table V: Analogs used to compute particle characteristics.		
Variable	Analog*	Definition
d_s	Area-equivalent diameter, x_{area}	$\sqrt{4A_p/\pi}$, where A_p is projected area of particle
F_s	Width-to-length ratio, F_w	c/a
P	Krumbein roundness, P_k	See Krumbein (1941); Wadell (1935)

* As measured by the Retsch *Camsizer XT*.

7 References

ACAROGLU, E. R. 1968. *Sediment Transport in Conveyance Systems.* Ph.D., Cornell University.

ADAMS, J. W. F., FAIRWEATHER, M. AND YAO, J. 2011. Particle deposition in circular pipes with variable bed height. *J. Phys. Conf. Ser.,* 318, 052001 (6 p.).

ANDREOTTI, B. AND CLAUDIN, P. 2013. Aeolian and subaqueous bedforms in shear flows. *Philos. Trans. A Math. Phys. Eng. Sci.,* 371, 20120364 (15 p.).

BAAS, J. H. 1993. *Dimensional analysis of current ripples in recent and ancient depositional environments.* Ph.D., Utrecht University.

BAAS, J. H. 1994. A flume study on the development and equilibrium morphology of current ripples in very fine sand. *Sedimentology,* 41, 185-209.

BAAS, J. H., BEST, J. L. AND PEAKALL, J. 2016. Predicting bedforms and primary current stratification in cohesive mixtures of mud and sand. *J. Geol. Soc.,* 173, 12-45.

BANASIAK, R. AND TAIT, S. 2008. The reliability of sediment transport predictions in sewers: influence of hydraulic and morphological uncertainties. *Water Sci. Technol.,* 57, 1317-1327.

BANASIAK, R. AND VERHOEVEN, R. 2008. Transport of sand and partly cohesive sediments in a circular pipe run partially full. *J. Hydraul. Eng.-ASCE,* 134, 216-224.

BEST, J. 2005. The fluid dynamics of river dunes: A review and some future research directions. *J. Geophys. Res.-Earth,* 110, F04S02 (21 p.).

CHARRU, F. 2006. Selection of the ripple length on a granular bed sheared by a liquid flow. *Phys. Fluids,* 18, 121508 (9 p.).

CHARRU, F., ANDREOTTI, B. AND CLAUDIN, P. 2013. Sand ripples and dunes. *Annu. Rev. Fluid Mech.,* 45, 469-493.

CHARRU, F. AND HINCH, E. J. 2006. Ripple formation on a particle bed sheared by a viscous liquid. Part 1. Steady flow. *J. Fluid Mech.,* 550, 111-121.

CHARRU, F. AND MOUILLERON-ARNOULD, H. 2002. Instability of a bed of particles sheared by a viscous flow. *J. Fluid Mech.,* 452, 303-323.

CLARK, A. H., SHATTUCK, M. D., OUELLETTE, N. T. AND O'HERN, C. S. 2015. Onset and cessation of motion in hydrodynamically sheared granular beds. *Phys. Rev. E,* 92, 042202 (7 p.).

COLEMAN, S. E. AND ELING, B. 2000. Sand wavelets in laminar open-channel flows. *J. Hydraul. Res.,* 38, 331-338.

COLEMAN, S. E., FEDELE, J. J. AND GARCÍA, M. H. 2003. Closed-conduit bed-form initiation and development. *J. Hydraul. Eng.-ASCE,* 129, 956-965.

COLEMAN, S. E. AND MELVILLE, B. W. 1994. Bed-form development. *J. Hydraul. Eng.-ASCE,* 120, 544-560.

COLEMAN, S. E. AND NIKORA, V. I. 2011. Fluvial dunes: initiation, characterization, flow structure. *Earth Surf. Proc. Land.,* 36, 39-57.

COLOMBINI, M. AND STOCCHINO, A. 2011. Ripple and dune formation in rivers. *J. Fluid Mech.,* 673, 121-131.

COREY, A. T. 1949. *Influence of shape on the fall velocity of sand grains.* MS, Colorado A&M College.

DIETRICH, W. E. 1982. Settling velocity of natural particles. *Water Resour. Res.,* 18, 1615-1626.

DXO LABS. unknown year. *Nikon AF Micro-Nikkor 60mm f/2.8D mounted on Nikon D810 :*

Tests and Reviews [Online]. Available: https://www.dxomark.com/Lenses/Nikon/Nikon-AF-Micro-Nikkor-60mm-F28D-mounted-on-Nikon-D810__963 [Accessed 2017].

EDELIN, D., JOSSET, C., CASTELAIN, C. AND FAYOLLE, F. 2015. Experimental study of bedforms obtained with floating particles in a pipe flow. *J. Fluid Mech.,* 765**,** 252-272.

ENGELUND, F. AND FREDSØE, J. 1970. Instability of erodible beds. *J. Fluid Mech.,* 42**,** 225-244.

ENGELUND, F. AND FREDSØE, J. 1982. Sediment ripples and dunes. *Annu. Rev. Fluid Mech.,* 14**,** 13-37.

FOURRIÈRE, A., CLAUDIN, P. AND ANDREOTTI, B. 2010. Bedforms in a turbulent stream: formation of ripples by primary linear instability and of dunes by nonlinear pattern coarsening. *J. Fluid Mech.,* 649**,** 287-328.

GAO, P. 2008. Transition between two bed-load transport regimes: Saltation and sheet flow. *J. Hydraul. Eng.-ASCE,* 134**,** 340-349.

GARCÍA, M. H. (ed.) 2008. *Sedimentation Engineering: Process, Measurements, Modeling and Practice,* Reston, Virginia: American Society of Civil Engineers.

GILLIES, R. G., SHOOK, C. A. AND XU, J. H. 2004. Modelling heterogeneous slurry flows at high velocities. *Can. J. Chem. Eng.,* 82**,** 1060-1065.

GORE, R. A. AND CROWE, C. T. 1989. Effect of particle size on modulating turbulent intensity. *Int. J. Multiphas. Flow,* 15**,** 279-285.

GORE, R. A. AND CROWE, C. T. 1991. Modulation of turbulence by a dispersed phase. *J. Fluid. Eng.-T. ASME,* 113**,** 304-307.

GRAF, W. H. 1984. *Hydraulics of Sediment Transport,* New York, Water Resources Publications.

HINZE, J. O. 1959. *Turbulence: an introduction to its mechanism and theory,* New York, McGraw-Hill.

HUNTER, T. N., PEAKALL, J., UNSWORTH, T. J., ACUN, M. H., KEEVIL, G., RICE, H. AND BIGGS, S. 2013. The influence of system scale on impinging jet sediment erosion: Observed using novel and standard measurement techniques. *Chem. Eng. Res. Des.,* 91**,** 722-734.

ISMAIL, H. M. 1952. Turbulent transfer mechanism and suspended sediment in closed channels. *Trans. Am. Soc. Civ. Eng.,* 117**,** 409-434.

JULIEN, P. Y. AND KLAASSEN, G. J. 1995. Sand-dune geometry of large rivers during floods. *J. Hydraul. Eng.-ASCE,* 121**,** 657-663.

KENNEDY, J. F. 1963. The mechanics of dunes and antidunes in erodible-bed channels. *J. Fluid Mech.,* 16**,** 521-544.

KIDANEMARIAM, A. G. AND UHLMANN, M. 2014. Interface-resolved direct numerical simulation of the erosion of a sediment bed sheared by laminar channel flow. *Int. J. Multiphas. Flow,* 67**,** 174-188.

KLEINHANS, M. G., LEUVEN, J. R. F. W., BRAAT, L. AND BAAR, A. 2017. Scour holes and ripples occur below the hydraulic smooth to rough transition of movable beds. *Sedimentology***,** DOI: 10.1111/sed.12358.

KRIEGEL, E. AND BRAUER, H. 1966. *Hydraulischer Transport körniger Feststoffe durch waagerechte Rohrleitungen,* Düsseldorf, VDI-Verlag.

KRUMBEIN, W. C. 1941. Measurement and geological significance of shape and roundness of sedimentary particles. *J. Sediment. Res.,* 11**,** 64-72.

KURU, W. C., LEIGHTON, D. T. AND MCCREADY, M. J. 1995. Formation of waves on a horizontal erodible bed of particles. *Int. J. Multiphas. Flow,* 21**,** 1123-1140.

LANGE, R. L. AND WICHERN, M. 2013. Sedimentation dynamics in combined sewer systems. *Water Sci. Technol.,* 68**,** 756-762.

LEEDER, M. 2011. *Sedimentology and Sedimentary Basins: From Turbulence to Tectonics,*

Oxford, Wiley-Blackwell.

MALARKEY, J., BAAS, J. H., HOPE, J. A., ASPDEN, R. J., PARSONS, D. R., PEAKALL, J., PATERSON, D. M., SCHINDLER, R. J., YE, L. P., LICHTMAN, I. D., BASS, S. J., DAVIES, A. G., MANNING, A. J. AND THORNE, P. D. 2015. The pervasive role of biological cohesion in bedform development. *Nat. Commun.,* 6**,** 6257 (6 p.).

MATOUŠEK, V. 2005. Research developments in pipeline transport of settling slurries. *Powder Technol.,* 156**,** 43-51.

MCLEAN, S. R., NELSON, J. M. AND WOLFE, S. R. 1994. Turbulence structure over two-dimensional bed forms: implications for sediment transport. *J. Geophys. Res.-Oceans,* 99**,** 12729-12747.

NAKAGAWA, H. AND TSUJIMOTO, T. 1984. Spectral analysis of sand bed instability. *J. Hydraul. Eng.-ASCE,* 110**,** 467-483.

OURIEMI, M., AUSSILLOUS, P. AND GUAZZELLI, E. 2009. Sediment dynamics. Part 2. Dune formation in pipe flow. *J. Fluid Mech.,* 636**,** 321-336.

OURIEMI, M., AUSSILLOUS, P., MEDALE, M., PEYSSON, Y. AND GUAZZELLI, E. 2007. Determination of the critical Shields number for particle erosion in laminar flow. *Phys. Fluids,* 19**,** 061706 (4 p.).

OURIEMI, M., CHAUCHAT, J., AUSSILLOUS, P., MEDALE, M. AND GUAZZELLI, E. 2010. Sediment transport and dunes in pipe flow. *"ICMF 2010", 7th International Conference on Multiphase Flow.* Tampa, Florida.

PEAKALL, J., ASHWORTH, P. AND BEST, J. 1996. Physical modelling in fluvial geomorphology: principles, applications and unresolved issues. *In:* RHOADS, B. AND THORN, C. (eds.) *The Scientific Nature of Geomorphology.* Chichester, UK.: Wiley.

PEYSSON, Y., OURIEMI, M., MEDALE, M., AUSSILLOUS, P. AND GUAZZELLI, E. 2009. Threshold for sediment erosion in pipe flow. *Int. J. Multiphas. Flow,* 35**,** 597-600.

POWERS, M. C. 1953. A new roundness scale for sedimentary particles. *J. Sediment. Res.,* 23**,** 117-119.

RAUDKIVI, A. J. 1963. Study of sediment ripple formation. *J. Hydr. Div.-ASCE,* 89**,** 15-33.

RAUDKIVI, A. J. 1976. *Loose Boundary Hydraulics,* Rotterdam, Pergamon Press.

RAUDKIVI, A. J. 1997. Ripples on stream bed. *J. Hydraul. Eng.-ASCE,* 123**,** 58-64.

RICE, H. P., FAIRWEATHER, M., PEAKALL, J., HUNTER, T. N., MAHMOUD, B. AND BIGGS, S. R. 2015a. Constraints on the functional form of the critical deposition velocity in solid-liquid pipe flow at low solid volume fractions. *Chem. Eng. Sci.,* 126**,** 759-770.

RICE, H. P., FAIRWEATHER, M., PEAKALL, J., HUNTER, T. N., MAHMOUD, B. AND BIGGS, S. R. 2015b. Measurement of particle concentration in horizontal, multiphase pipe flow using acoustic methods: Limiting concentration and the effect of attenuation. *Chem. Eng. Sci.,* 126**,** 745-758.

RICHARDS, K. J. 1980. The formation of ripples and dunes on an erodible bed. *J. Fluid Mech.,* 99**,** 597-618.

SIMKHIS, M., BARNEA, D. AND TAITEL, Y. 1999. Dunes in solid-liquid flow in pipes. *Hydrotransport 14.* Maastricht: BHR Group.

SIMONS, D. B. AND RICHARDSON, E. V. 1961. Forms of bed roughness in alluvial channels. *J. Hydr. Div.-ASCE,* 87**,** 87-105.

SKIPWORTH, P. J., TAIT, S. J. AND SAUL, A. J. 1999. Erosion of sediment beds in sewers: Model development. *J. Environ. Eng.-ASCE,* 125**,** 566-573.

SOULSBY, R. 1997. *Dynamics of Marine Sands: A Manual for Practical Applications,* London, Thomas Telford.

SUMER, B. M. AND BAKIOGLU, M. 1984. On the formation of ripples on an erodible bed. *J. Fluid Mech.,* 144**,** 177-190.

SYVITSKI, J. P. M. E. 2007. *Principles, Methods and Application of Particle Size Analysis,* Cambridge, Cambridge University Press.

TAKAHASHI, H., MASUYAMA, T. AND NODA, K. 1989. Unstable flow of a solid-liquid mixture in a horizontal pipe. *Int. J. Multiphas. Flow,* 15**,** 831-841.

THOMAS, D. G. 1964. Periodic phenomena observed with spherical particles in horizontal pipes. *Science,* 144**,** 534-536.

VAN RIJN, L. C. 1984a. Sediment transport, part I: bed load transport. *J. Hydraul. Eng.-ASCE,* 110**,** 1431-1456.

VAN RIJN, L. C. 1984b. Sediment transport, part II: suspended load transport. *J. Hydraul. Eng.-ASCE,* 110**,** 1613-1641.

VAN RIJN, L. C. 1984c. Sediment transport, part III: bed forms and alluvial roughness. *J. Hydraul. Eng.-ASCE,* 110**,** 1733-1754.

VAN RIJN, L. C. 1989. *Handbook sediment transport by currents and waves,* Delft, Delft Hydraulics.

WADELL, H. 1935. Volume, shape, and roundness of quartz particles. *J. Geol.,* 43**,** 250-280.

WILSON, K. C. 1965. Derivation of the regime equations from relationships for pressurized flow by use of the principle of minimum energy - degradation rate, Civil Engineering Research Report No. 51. Kingston, Ontario: Queen's University.

YALIN, M. S. 1972. *Mechanics of sediment transport,* Oxford, Pergamon Press.